

Using a multi-omics approach to
understand the drivers of proteasome
inhibitor resistance in multiple myeloma,
and using epigenetic inhibitors to
identify mechanisms of reversing the
resistance



Anna James-Bott

St Hilda's College

Nuffield Department of Orthopaedics,
Rheumatology and Musculoskeletal Sciences

University of Oxford

A thesis submitted for the degree of

Doctor of Philosophy

Trinity 2021

Acknowledgements

I would like to thank my supervisors Dr Adam Cribbs, Professor Udo Oppermann and Dr Sarah Gooding etc etc...

GSK... DTC... Family... Friends...

Abstract

Multiple myeloma (MM) is an incurable cancer of plasma cells, with an average five-year survival rate of approximately 50%. More novel therapeutics, namely proteasome inhibitors (PI) and immunomodulatory imide drugs, have almost doubled median survival time of MM patients. However, most patients relapse and become resistant to drugs they previously have been treated with. Acquired anti-cancer drug resistance remains one of the biggest barriers in the treatment of myeloma. Recently, epigenetic mechanisms have been implicated in both the onset of MM and in the development of drug resistance. This thesis aims to investigate the changes that drive proteasome inhibitor drug resistance and to identify epigenetic compounds capable of reversing the resistance phenotype, and characterise their mechanism of action.

Following an epigenetic compound library screen and bulk RNA-seq, a dual TRIM24/BRPF inhibitor (TRIM24i) was selected to be investigated further as it was shown to kill carfilzomib-resistant AMO-1 cells (aCFZ) in the presence of carfilzomib but had little effect on PI-sensitive (WT) AMO-1 cells, demonstrating that it is capable of re-sensitizing carfilzomib-resistant AMO-1 cells to carfilzomib. Transcriptomic, epigenomic and proteomic changes were studied using an array of 'omic' techniques, including bulk and single-cell RNA-Seq, phosphoproteomics, ubiquitinomics, total proteomics, CyTOF and ChIP-Seq (PROBABLY will at some point).

Contents

List of Figures	viii
List of Tables	ix
List of Abbreviations	x
1 Introduction	1
1.1 Overview	1
1.2 The adaptive immune system	1
1.2.1 Plasma cells	2
1.3 Multiple myeloma	3
1.3.1 Multiple myeloma cells	3
1.3.2 Epidemiology	3
1.3.3 Presentation	4
1.3.4 Treatment of multiple myeloma	5
1.3.5 Proteasome inhibitors	5
1.4 Drug resistance in multiple myeloma	7
1.5 Transcriptomics, proteomics and epigenomics	7
1.5.1 The genome	8
1.5.2 The transcriptome	9
1.5.3 The proteome	9
1.5.4 The epigenome	10
1.5.5 RNA-Seq	10
1.5.6 ATAC-seq	11
1.5.7 ChIP-Seq	11
1.5.8 Next generation sequencing	11
1.5.9 CyTOF	12
1.5.10 Liquid chromatography with tandem mass spectrometry . .	12
1.6 Summary	12
1.7 Aims	12

2	Background	14
2.1	Drug resistance in MM	14
2.1.1	Genomic changes in drug resistant MM	14
2.1.2	Epigenetic changes in drug resistant MM	14
2.2	Preliminary work	14
2.2.1	Epigenetic compound library screen	14
3	Methods	17
3.1	Cell culture	17
3.1.1	AMO-1 cells	17
3.2	Compounds	17
3.2.1	Proteasome inhibitors	17
3.2.2	Epigenetic inhibitors	18
3.3	Assays	18
3.3.1	Cell viability assays	18
3.3.2	Dose response curves	18
3.4	Bulk RNA-seq	19
3.4.1	RNA extraction	19
3.4.2	RNA library preparation	19
3.5	Single-cell RNA-seq	20
3.5.1	Cell encapsulation	20
3.5.2	Library preparation	20
3.6	ATAC maybe	20
3.6.1	ATAC stuff	20
3.7	ChIP maybe	20
3.7.1	ChIP stuff	20
3.8	Sequencing	20
3.9	Phosphoproteomics	20
3.9.1	Collecting cell pellets	20
3.9.2	Cell lysis	21
3.9.3	Protein quantification	21
3.9.4	Protein Digestion	21
3.9.5	Peptide purification	22
3.10	Ubiquitinomics	22
3.10.1	Collecting cell pellets	22
3.10.2	Cell lysis	23
3.10.3	Protein quantification	23
3.10.4	Protein Digestion	23
3.10.5	Peptide purification	23

3.10.6	Immunoaffinity purification	24
3.11	Liquid-chromatography-tandem mass spectrometry	24
3.12	Data Processing	25
3.12.1	Bulk RNA-Seq	25
3.12.2	Single-cell RNA-Seq	25
3.12.3	LC-MS/MS	25
3.13	CyTOF	26
3.13.1	CyTOF stuff	26
4	Workflow Generation	27
4.1	Introduction	27
4.1.1	Reproducible workflows	27
4.1.2	Computational pipelines	28
4.2	scRNA-Seq pseudoalignment pipeline	28
4.2.1	Pseudoalignment	28
4.2.2	Benchmark	30
4.3	scRNA-Seq velocity analysis pipeline	36
4.3.1	RNA velocity	36
5	Identifying a lead epigenetic compound	37
5.1	Identifying inhibitors of interest	37
5.1.1	Bulk RNA-seq	37
5.1.2	Dose response curves	39
6	Multi-omics characterisation of PI resistance in AMO-1 cells	41
6.1	Introduction	41
6.2	Results	42
6.2.1	Transcriptional changes	42
6.2.2	Phosphoproteomics	43
6.2.3	Ubiquitinomics	43
Appendices		
A	Epigenetic compound screen	49
References		50

List of Figures

1.1	Hematopoietic system cell differentiation	2
1.2	Structure of the proteasome	8
1.3	Drop-seq schematic	11
2.1	Epigenetic compound library pie chart	15
2.2	Epigenetic compound library screen	16
3.1	TRIM24i structure	18
4.1	scRNA-Seq pseudoalignment pipeline flowchart	30
4.2	Benchmark Salmon Alevin Knee Plot	32
4.3	Benchmark Kallisto Bus Rotated Knee Plot	33
4.4	F1, Precision and Recall Bar Charts	34
4.5	Distribution of F1 scores	34
4.6	Benchmark Clustering Analysis	35
5.1	Bulk RNA-Seq WT and aCFZ cells epigenetic treated PCA	38
5.2	Dose response curves	40
5.3	PI dose response curve: aCFZ pretreated with TRIM24i	40
6.1	WT, aCFZ and TRIM24i reversal, transcriptomics differential ex- pression and clustering	43
6.2	Transcription factor heatmap	44
6.3	Transcription factor venn diagrams WT, aCFZ control and aCFZ TRIM24i treated	45
6.4	Phosphoproteomics PCA	46
6.5	Ubiquitinomics PCA	47

List of Tables

1.1	Timeline of treatment options for multiple myeloma	6
4.1	Carol diagram of true/false positives/negatives based on expression between predicted values by Alevin/BUS and the ground truth matrix.	33
5.1	AMO-1 cells proteasome inhibitor IC_{50} s	39

List of Abbreviations

MM	Multiple Myeloma
BM	Bone marrow
MGUS	Monoclonal gammopathy of unknown significance
SMM	Smoldering multiple myeloma
PI	Proteasome inhibitor
IMiDs	Immunomodulatory imide drugs
ER	Endoplasmic reticulum
UPS	Ubiquitin proteasome system
UPR	Unfolded protein response
DNA	Deoxyribonucleic acid
RNA	Ribonucleic acid
NGS	Next generation sequencing
WGS	Whole genome sequencing
RNA-Seq	. . .	Ribonucleic acid sequencing
scRNA-Seq	. .	Single cell RNA-Seq
dscRNA-Seq	. .	Droplet-based scRNA-Seq
CB	Cellular barcode
UMI	Unique molecular identifier
LC-MS/MS	. .	Liquid chromatography with tandem mass spectrometry
PCA	Principle component analysis
DMSO	Dimethyl sulfoxide
UMAP	Uniform Manifold Approximation and Projection
tSNE	t-distributed Stochastic Neighbor Embedding

Introduction

1.1 Overview

...

1.2 The adaptive immune system

Humans are exposed to millions of potential pathogens every day and therefore require defences to be able to protect themselves against infection. These defences can be innate or adaptive. An example of an innate defence is the skin acting as a physical barrier between the outside world and the body. Another example of an innate defence is non-specific engulfing (phagocytosis) of foreign pathogens by macrophages (a type of white blood cell). Innate responses are relied upon as the first line of defence, however sometimes a more sophisticated, specialised response is required- called the adaptive immune response. (REF-mol biology of the cell).

Adaptive immune responses are specific to the pathogen that induced the response and are dependent on B cells and T cells, two major classes of lymphocytes (a class of white blood cell). Two classes of adaptive immune responses exist: antibody responses, co-ordinated by B cells, and cell mediated immune responses, co-ordinated by T cells. T-cell-mediated immune responses recognise foreign antigens (antibody generators; substances capable of eliciting an immune response by stimulating B or T cell activation) on the surface of cells and can either kill the pathogen-infected cells or stimulate B cells or phagocytes to help eliminate the pathogen.

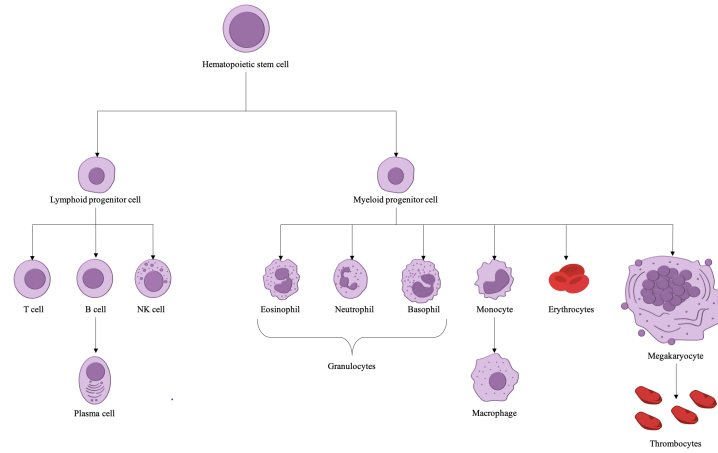


Figure 1.1: Hematopoietic stem cell (HSC) cell differentiation. HSCs divide into myeloid or lymphoid progenitor cells. Dendritic cells and a number of precursor states have been omitted.

In antibody responses, B cells and plasma cells secrete antibodies, also known as immunoglobulins. Immunoglobulins are large Y-shaped proteins, which recognise and bind to the specific foreign antigen on the pathogen which stimulated their production. Binding of immunoglobulins to antigens renders the virus or microbial toxin inactive as it blocks their ability to bind to host cells. Additionally, antibody binding makes it easier for phagocytic cells to ingest the pathogen.

1.2.1 Plasma cells

Plasma cell development

Stem cells are precursor cells which can give rise to at least one type of differentiated (mature) cell, with the capability of indefinite self-renewal. Hematopoietic stem cells (HSC) are stem cells that give rise to all the cells of the hematopoietic system. Two predominant cell populations are produced by HSCs: the common myeloid progenitor (CMP) and the common lymphocyte progenitor (CLP). CMP differentiation produces erythrocytes (red blood cells), mast cells, monocytes, macrophages, neutrophils, eosinophils, basophils and myeloid dendritic cells. CLP differentiation results in B cells, T cells, natural killer (NK) cells and lymphoid dendritic cells.

Most B cells die in the bone marrow soon after developing, however some will develop in the bone marrow, where initial stages of maturation occur and then migrate to secondary lymphoid organs, such as the spleen. Within secondary lymphoid organs, numerous critical decisions on B cell fate are made, involving complex transcriptional networks, cell interactions, gene rearrangements, and mutations[1, 2]. Upon antigenic-stimulation, naive B cells differentiate into memory B cells or plasma cells. Terminally differentiated plasma cells are the final effectors of the B cell lineage, each dedicated to secreting large amounts of a single type of antibody. Plasma cells have an extensive rough endoplasmic reticulum (ER), and have numerous genes involved in immunoglobulin secretion upregulated, including *XBP-1* and *CHOP*[3], to enable the production of copious amounts of antibody. Plasma cells appear to consist of two distinct categories: short-lived plasma cells, which have life-spans of several months and are located in extrafollicular locales such as in medullary chords of lymph nodes or the red pulp of the spleen, and long-lived plasma cells, which have life-spans of decades and are mainly found in the bone marrow[4, 5].

1.3 Multiple myeloma

1.3.1 Multiple myeloma cells

Multiple myeloma is a malignancy of terminally differentiated plasma cells. It is characterised by aberrant proliferation of clonal, long-lived plasma cells in the bone marrow[6].

1.3.2 Epidemiology

Multiple myeloma accounts for 1-2% of all cancers and has the second highest incidence of hematological malignancies, after non-Hodgkin's lymphoma[7]. MM is rare in individuals under the age of 40, with the average age at time of diagnosis centering around 70[8, 9]. MM is more prevalent in males than females and is around twice as common in black populations than in Caucasian or Asian populations[10]. The average incidence rate is approximately 1-6 cases per 100000 individuals[8, 9,

11], with the highest age-standardised incidence rates in the regions of Australasia, North America, and Western Europe[12]. Five-year survival rate of MM patients is approximately 49%, whilst approximately a third of MM patients survive ten years or greater[13, 14].

1.3.3 Presentation

Precursor states

All cases of MM are preceded by asymptomatic precursor states, monoclonal gammopathy of unknown significance (MGUS) and smoldering multiple myeloma (SMM). However, only some patients with SMM or MGUS progress to active MM.

MGUS is a pre-malignant condition where patients have the presence of monoclonal immunoglobulins in their blood or urine, $<10\%$ clonal plasma cells in their bone marrow, but lack any myeloma-related end-organ damage[15]. Patients with SMM have between 10 and 60% clonal plasma cells in their bone marrow, serum monoclonal immunoglobulin of ≥ 3 g/dL, and like MGUS, have no signs of end-organ damage[16]. Progression risk of MGUS into symptomatic MM is about 1% per year, whilst progression risk of SMM to MM is higher, at around 10% per year for the first 5 years, after which it decreases[17, 18].

Active MM

There are multiple classifications of active MM. The International Myeloma Working Group's definition[19] is as follows: Greater than 10% clonal plasma cells located in the bone marrow and one or more myeloma-defining event or biomarker of malignancy. Myeloma defining events consist of evidence of end-organ damage that can be attributed to the surplus of M protein and clonal plasma cells, namely the CRAB features:

- Hypercalcemia
 - Serum calcium > 1 mg/dL higher than the upper limit of normal, or
 - Serum calcium > 11 mg/dL

- Renal insufficiency
 - Creatinine clearance < 40 mL per min, or
 - Serum creatine > 2 mg/dL
- Anemia
 - Hemoglobin value of > 20 g/L below the lower limit of normal, or
 - Hemoglobin value < 100 g/L
- Bone lesions
 - One or more osteolytic lesions on skeletal radiography, CT or PET-CT

Biomarkers of malignancy include greater than or equal to 60% clonal plasma cells in the bone marrow, an involved:uninvolved serum free light chain ratio greater than or equal to 100, and more than one focal lesion on an MRI study[19].

It is currently unclear what causes the malignant transformation between precursor states and active MM. However certain factors have been identified as risk factors, including point mutations, a large array of up-regulated transcription factors, and numerous immune events.

1.3.4 Treatment of multiple myeloma

Multiple myeloma may be an incurable disease, however it is treatable. In fact, in the last decade median survival time for newly diagnosed MM patients has almost doubled[20]. Novel therapeutic advances have contributed to this improvement (Table1.1).

1.3.5 Proteasome inhibitors

Proteasome inhibitors have contributed greatly to the improved prognosis of MM since their introduction into treatment regimes. The first-in-class proteasome inhibitor bortezomib (Velcade[®]) was approved by the FDA in 2003 as a single-agent for injection of relapsed MM[28]. Since then it has been approved for use

Year	Treatment	Usage	Ref
1958	Melphalan	The alkylating agent melphalan was first used in plasma cell myeloma in 1958.	[21]
1960s	Corticosteroids	Placebo-controlled double-blind trial of prednisone in multiple myeloma. Combinations of prednisone and melphalan showed an increased survival over melphalan alone. Dexamethasone and prednisone have become a cornerstone in the treatment of multiple myeloma.	[22, 23]
1980s	Stem-cell transplantations	Numerous successful allogenic and autologous bone marrow transplantations in patients with multiple myeloma	[24–27]
2003	Proteasome inhibitors	Bortezomib, a first-in-class proteasome inhibitor, was first approved by the FDA for use in relapsed and refractory multiple myeloma. In 2008 it was approved for patients with no prior treatment. Carfilzomib was approved in 2012 for advanced MM and later in 2015 for treatment of relapsed MM. The oral proteasome inhibitor, ixazomib, was approved as a combination treatment with lenalidomide and dexamethasone in 2016 for people who have received at least one previous treatment.	[28–30]
2006	IMiDs	The antitumour activity of thalidomide was demonstrated in 1999, this led to the development of lenalidomide, the first approved immunomodulatory imide drug (IMiD) for use in multiple myeloma. Currently, thalidomide, lenalidomide and pomalidomide are approved for use in multiple myeloma	[31–33]
2015	Monoclonal antibodies	In 2015, daratumumab, an anti-CD38 monoclonal antibody and elotuzumab, an anti-SLAMF7 monoclonal antibody, were approved for MM treatment.	[34, 35]

Table 1.1: Timeline of treatment options for multiple myeloma. Listed by first usage or FDA approval for MM.

in combination therapies. Bortezomib in combination with melphalan-prednisone proved to be superior to the previous standard of care for patients ineligible for HDT-ASCT of melphalan-prednisone alone, increasing time until tumour progression[36]. The combination of bortezomib, dexamethasone and thalidomide was also shown to

be superior to previous standard of care for patients prior to ASCT[37]. In 2010, bortezomib was approved as a frontline therapy for treatment-naive MM patients. Since then, two more proteasome inhibitors have been approved, carfilzomib and ixazomib. Carfilzomib is structurally and mechanistically different to bortezomib and shows activity on bortezomib resistant primary MM cells[37]; it is approved for relapsed or refractory MM.

The ubiquitin-proteasome system

Proteasome inhibitors work by blocking the action of the proteasome in the cell. Misfolded proteins can be harmful to a cell, so the combined activity of molecular chaperones, which aid in protein folding, and the ubiquitin-proteasome system (UPS), which acts to digest misfolded proteins, is needed to prevent massive protein aggregation. Unneeded, misfolded or damaged proteins are tagged with lysine-48-linked poly-ubiquitin chains, marking them for degradation by the proteasome (Figure 1.2a). The proteasome is sometimes described as a complex ‘protein destruction machine’. The proteasome consists of the 20S core particle, a central hollow cylinder, and the 19S regulatory caps associated with each end of the cylinder. The 19S regulatory caps perform substrate recognition, deubiquitination, unfolding and threading of the protein substrate into the 20S core. The core is made up of four stacked heptameric ring structures. The outer rings are responsible for docking to the 19S cap and for acting as a gate to the inner rings. The inner rings consist of seven β subunits, containing inward-facing protease active sites for degrading proteins[38, 39] (Figures 1.2a and 1.2b).

1.4 Drug resistance in multiple myeloma

... Lit review??

1.5 Transcriptomics, proteomics and epigenomics

It has been shown that changes in the genome, transcriptome, epigenome and proteome all contribute to acquired-drug resistance in myeloma. Therefore, to

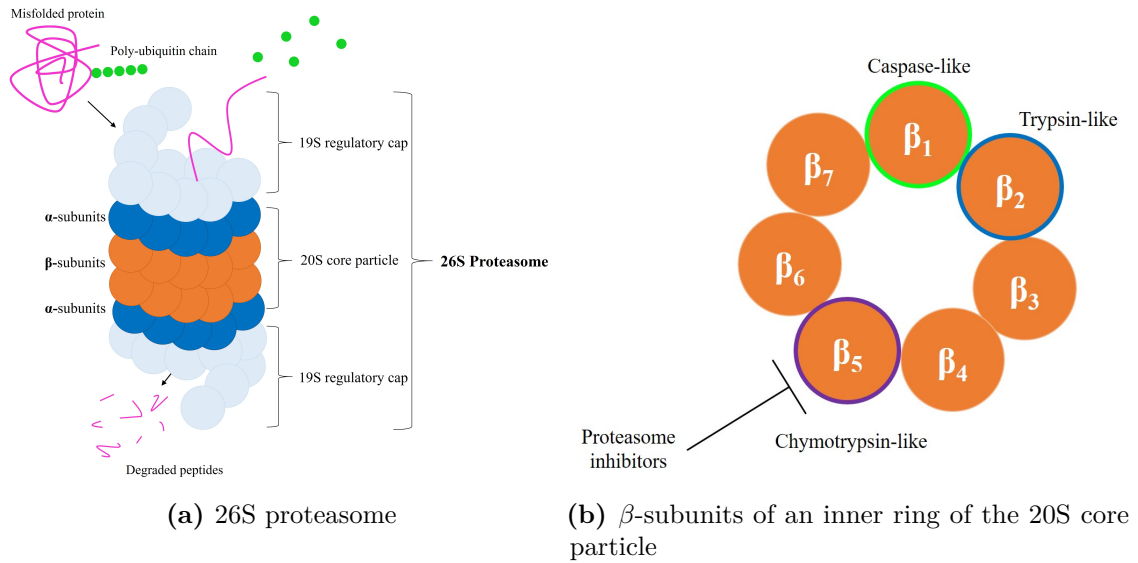


Figure 1.2: Structure of the proteasome. 1.2a shows the structure of the 26S proteasome, comprised of the 19S regulatory caps and 20S core particle. A misfolded protein tagged with a poly-ubiquitin chain is recognised by the 19s regulatory cap, which cleaves the ubiquitins from the protein and threads the protein through to the core, where it is degraded into small peptides. The 20S core particle is made up of two outer rings of α -subunits and two inner rings of β -subunits. 1.2b shows the β -subunit arrangement in one of the inner rings of the 20s particle. β_1 (caspase-like), β_2 (trypsin-like) and β_5 (chymotrypsin-like) are the proteolytically active subunits. Proteasome inhibitors are designed to primarily inhibit β_5 .

sufficiently investigate the multiple layers driving this development of resistance, a multi-omics approach must be employed.

1.5.1 The genome

The genome is the genetic material of an organism, it consists of deoxyribonucleic acid (DNA). DNA consists of two polynucleotide chains (or strands), running anti-parallel to each other, held together in a double helix structure by hydrogen bonds. Nucleotides are composed of a five-carbon sugar (deoxyribose for DNA), attached to one or more phosphate group (a single phosphate group in the case of DNA) and a nitrogenous base. Nucleotides are covalently linked to form an alternating sugar-phosphate backbone, with bases extending from each sugar towards the inside of the double helix. Nucleotides contain four different types of bases: adenine (A), cytosine (C), guanine (G) and thymine (T). The two DNA chains are held together by hydrogen bonds via complementary base pairing between the bases of the strands,

A pairing with T and G pairing with C. Often sections of DNA are denoted as their sequence of A, C, T and Gs (in order reading from the 5' to 3' direction).

The complete genome is made up of coding DNA (genes), non-coding DNA, as well as mitochondrial DNA and ribosomal DNA. An alteration in the nucleotide sequence of the genome is called a mutation. There are a number of types of mutations, including insertions, deletions, inversions, substitutions and duplications. A technique called whole genome sequencing (WGS) can be used to determine the sequence of nucleotides in an individual's DNA and therefore it can be used to determine any variations in the genome. However the technique is expensive and many experiments are interested in coding DNA only, so perform RNA-Seq to look at the transcriptome instead.

1.5.2 The transcriptome

Transcription is the first of many steps in gene expression. During transcription, the enzyme RNA polymerase reads a DNA sequence and produces an anti-parallel, complementary ribonucleic acid (RNA) strand. The transcriptome is the set of all RNA transcripts of an individual. RNA is a nucleic acid similar to DNA. Like DNA it has a sugar-phosphate backbone and 4 different types of bases attached to each sugar. However unlike DNA, RNA is single-stranded, it contains the sugar ribose in place of deoxyribose, and the nucleotide uracil (U) in place of thymine (T). There are many types of RNA, such as messenger RNA (mRNA), transfer RNA (tRNA), and ribosomal RNA (rRNA). RNA-seq is frequently used to study the transcriptome (outlined in section 1.5.5).

1.5.3 The proteome

Translation...

CyTOF and LC-MS/MS are often used to examine the proteome (section 1.5.9 and section 1.5.10).

1.5.4 The epigenome

Epigenetics is the study of any heritable phenotypic changes that do not involve alterations of the DNA sequence itself. [REF] ...

1.5.5 RNA-Seq

Modern RNA sequencing (RNA-Seq) implements next generation sequencing (NGS) technology to analyse RNA across the transcriptome of a biological sample and allows for the quantification of gene expression.

Bulk RNA-Seq

Bulk RNA-seq measures the average expression across a sample. Creating a bulk RNA-seq library involves isolating RNA from a biological sample, filtering for a specific type of RNA (most commonly mRNA), fragmentation of RNA into fragments, reverse transcription of the fragments to generate a complementary DNA (cDNA) library, end repair and adaptor ligation of the cDNA library, followed by PCR amplification ready for sequencing.

Single-cell RNA-Seq

Single-cell RNA-Seq (scRNA-Seq) measures gene expression for each individual cell across a population of cells and therefore provides information on clonal diversity that may be lost when pooling cells into bulk samples. Since its inception in 2009[40], there have been numerous scRNA-Seq techniques, such as SMART-seq2[41], Drop-seq[42], STRT[43] and inDrops[44]. scRNA-Seq library preparation shares many steps with bulk RNA-Seq workflow, however preliminary steps are required to isolate single cells and track them (??/ barcode) individually.

For droplet-based scRNA-Seq (dscRNA-seq) methods, single cells are isolated using microfluidic devices by individually encapsulating them in aqueous droplets contained in oil. Below, a dscRNA-seq method, Drop-seq, is outlined (Figure 1.3).

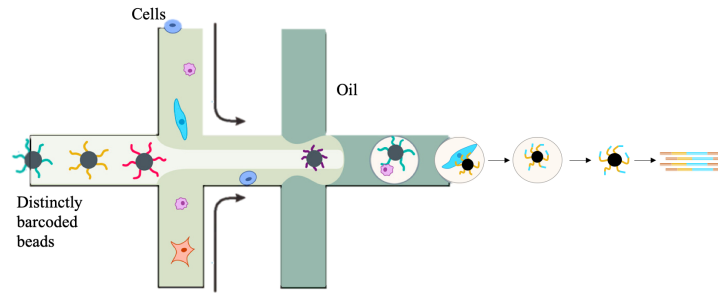


Figure 1.3: Outline of Drop-seq, a droplet-based scRNA-Seq method. Figure adapted from Macosko et al. (2015) [42]. A microfluidic device combines two aqueous flows, one containing cells and the other containing barcoded primer beads suspended in lysis buffer. The two aqueous channels flow across an oil channel to form aqueous droplets surrounded by oil. Relatively few droplets contain both a cell and a bead. Following droplet formation, the cell is lysed and its mRNAs are released, which then hybridise to the primers on the bead surface. A reagent is added to break up the droplets and the beads are collected and washed. The mRNAs are reverse-transcribed into cDNAs, generating a set of “STAMPS” (single-cell transcriptomes attached to microparticles) and template switching is used to introduce a PCR handle. The barcoded STAMPS can then be amplified using PCR.

1.5.6 ATAC-seq

...

1.5.7 ChIP-Seq

Chromatin immunoprecipitation sequencing (ChIP-seq) is used to analyse protein interactions with DNA. At a base-pair resolution, it is used to map DNA-binding proteins and histone modifications. Therefore ChIP-seq is often used to determine the mechanisms of gene regulation of transcription factors, and to study epigenetic mechanisms in detail.

1.5.8 Next generation sequencing

Next generation sequencing (NGS), differs from its predecessors in that it is highly scalable and massively parallel. With NGS you can rapidly sequence the entire genome if desired. It is quicker and cheaper than traditional Sanger sequencing, and progressed data output from the kilobase range up to potentially multiple terabases per run.

1.5.9 CyTOF

...

1.5.10 Liquid chromatography with tandem mass spectrometry

Liquid chromatography with tandem mass spectrometry (LC-MS/MS) based proteomics is a popular analytical technique to measure the protein abundance of a sample. The general steps for LC-MS/MS-based proteomics include: cell lysis, protein extraction, protein digestion using an enzyme to cleave proteins into peptides, peptide purification, and analysis by mass spectrometry. The resultant data includes mass and charge (m/z) information and peak intensities. Software is then employed which performs database searches and calculates the most likely peptide for each peak. From this data, protein abundance can then be calculated and normalised.

LC-MS/MS-based proteomics can also be used to search for specific proteins within the proteome. For example, immobilized metal affinity chromatography (IMAC) can be used to enrich for phosphorylated peptides (phosphoproteomics), and anti-ubiquitin antibodies can be used to enrich for ubiquitinated peptides (ubiquitinomics).

1.6 Summary

1.7 Aims

This thesis aims to characterise the changes driving proteasome-inhibitor resistance in multiple myeloma and identify possible mechanisms of reversing resistance. Chapter 2 gives background to the project, it reviews the literature surrounding drug resistance in MM and outlines preliminary work performed in the lab, that birthed this project. Chapter 3 outlines the methodology used in this work. Chapter 4 outlines the computational workflows generated to support this work and gives the results of a benchmark conducted to analyse the effectiveness of a computational pipeline developed. Chapter 5 describes how a lead epigenetic compounds

was selected, analysing results from bulk RNA-seq data and validating previous compound screen results with dose response curves. Chapter 6 delves deeper into the drivers of changes in drug resistance and the mechanism of action of TRIM24i on resistant cells by looking at an array of multi-omics data.

2

Background

2.1 Drug resistance in MM

2.1.1 Genomic changes in drug resistant MM

2.1.2 Epigenetic changes in drug resistant MM

2.2 Preliminary work

2.2.1 Epigenetic compound library screen

REMAKE FIGURE— LOADS OF SPELLING MISTAKES AND LOOKS AWFUL!!! Previously in the Oppermann group laboratory, Dr James Dunford performed a compound screen against WT and proteasome inhibitor-resistant AMO-1 cells with an epigenetic compound library (figure 2.1) and cell viability assays.

The results from the screen can be seen in figure 2.2. Six compounds, shown circled in red, were identified as compounds of interest. SGC-CBP30, TRIM24i, OF1 and GSK959 are bromodomain inhibitors, TMP269 is a HDAC inhibitor and TDOSI000054a (T54) is a methyl lysine binder. These compounds were of interest as they had little to no effect on WT cells and decreased cell viability of resistant cells in the presence of their respective proteasome inhibitor. This indicated that the compounds were not just killing cells with their own distinct mechanism of action, but instead seemed to be reversing proteasome inhibitor resistance and re-sensitising resistant AMO-1 cells to proteasome inhibitors. These compounds were then taken

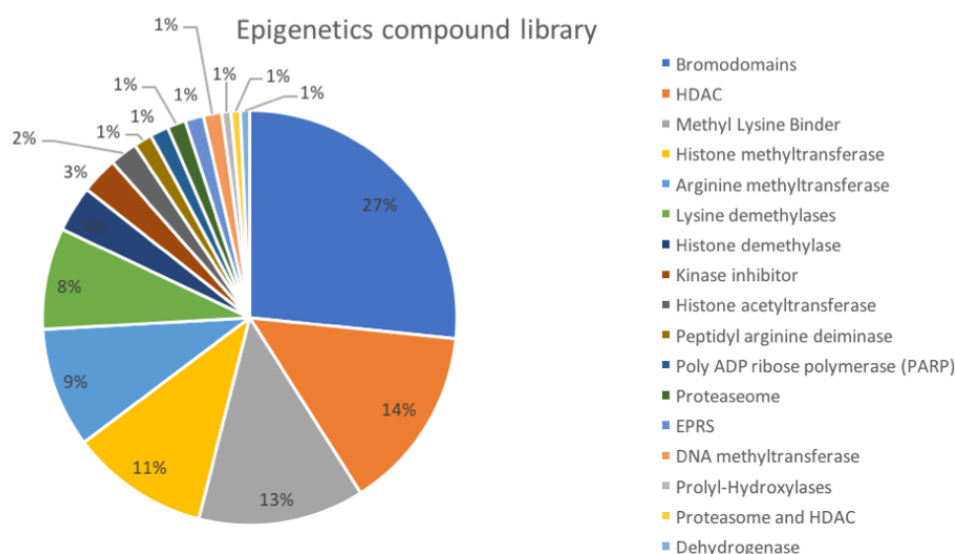


Figure 2.1: The Oppermann group epigenetic compound library. Proportions of targets in the 144-compound library.

forwards and used to treat carfilzomib resistant AMO-1 cells (aCFZ) and bulk RNA-seq perform to try and understand their mechanism of action.

Bromodomains (BRDs) are conserved modular protein-protein interaction domains. Primarily, BRDs recognise acetylated lysine (Lys) residues in histone tails. Proteins containing bromodomains are epigenetic regulators and regulate gene expression (on their own or as part of a larger complex) via chromatin remodelling, histone modification, histone recognition and transcriptional machinery regulation [REPHRASE]. Proteins containing BRDs have frequently been seen to be dysregulated in cancer. The compound SGC-TRIM24 is a dual inhibitor that targets the bromodomains of TRIM24 and BRPF.

(cite: <https://www.nature.com/articles/nrm.2016.143>)

Bromodomains are “readers” that bind acetylated lysines in histone tails

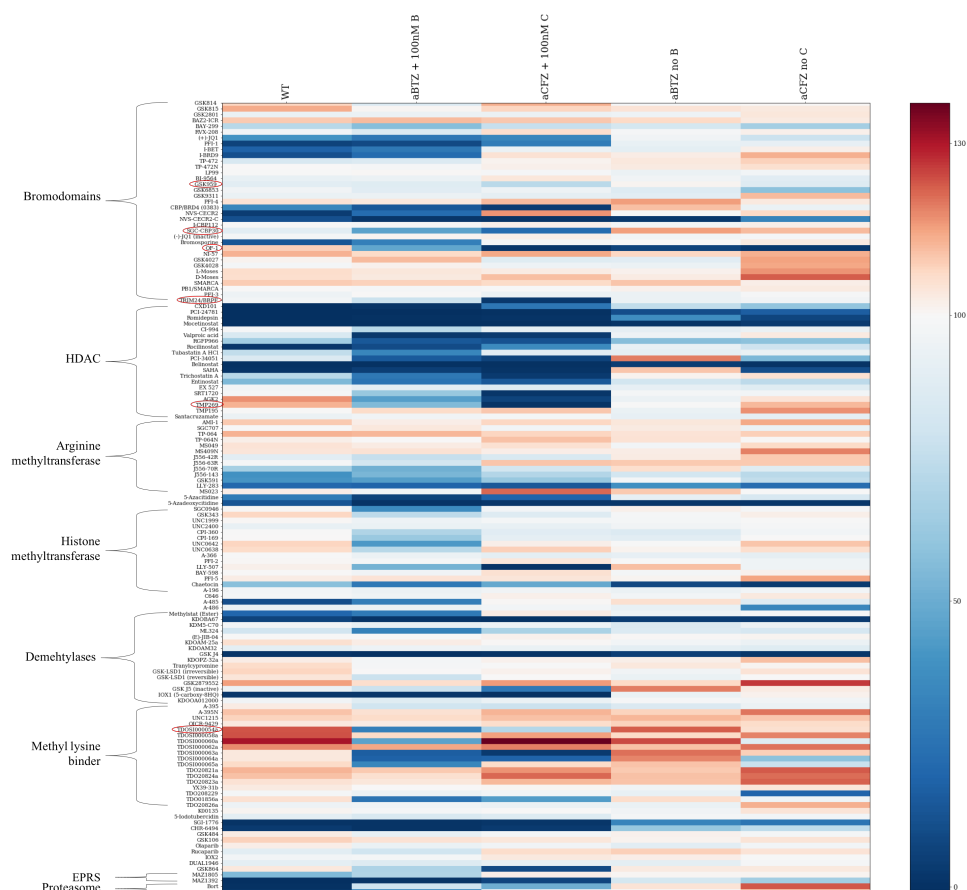


Figure 2.2: Preliminary epigenetic compound library screen, previously performed in the lab by Dr James Dunford. 138 epigenetic compounds were screened against proteasome inhibitor sensitive (WT) AMO-1 cells, carfilzomib resistant (aCFZ) and bortezomib resistant AMO-1 cells, in the presence of their respective proteasome inhibitor (+ 100nM B/C) and without (no B/C). Six compounds of interest were identified, circled in red in the figure.

3

Methods

3.1 Cell culture

3.1.1 AMO-1 cells

AMO-1 cells, plasma cells from a 64-year old female myeloma patient, were used as a model cell-line for multiple myeloma. Bortezomib and carfilzomib resistant AMO-1 cells were generated and kindly gifted by the Driessen lab[45]. Bortezomib, carfilzomib, pomalidomide and bortezomib plus pomalidomide resistant AMO-1 cells were also generated by Dr James Dunford by continual and escalating drug exposure of drug-sensitive (WT) cells. Carfilzomib and bortezomib resistant AMO-1 cells were kept in 100nM of their respective proteasome inhibitor and pomalidomide resistant AMO-1 cells were kept in 6 μ M pomalidomide. AMO-1 cells were cultivated in RPMI-1640 medium (Thermofisher, UK), supplemented with 10% fetal bovine serum (FBS), 100 μ g ml⁻¹ streptomycin and 100 U/ml penicillin (P/S) and 2mM L-glutamine (Invitrogen, UK). Cells were passaged when they reached approximately 1.5-2 million cells per ml. Media was replaced twice a week. AMO-1 cells are suspension cells.

3.2 Compounds

3.2.1 Proteasome inhibitors

<WHERE were they obtained> etc etc.

3.2.2 Epigenetic inhibitors

The Oppermann group has an epigenetic compound screening library, consisting of 144 compounds. The compounds were obtained XYZ <where did Jim get compounds> SGC???? A dual TRIM24/BRPF inhibitor was identified as a possible candidate to reverse drug-resistance in AMO-1 cells. The structure of the inhibitor is shown below in figure 3.1.

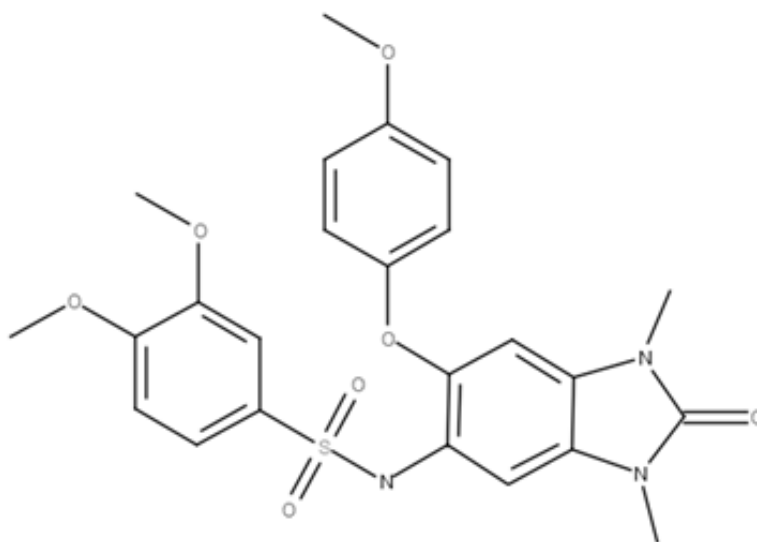


Figure 3.1: TRIM24 inhibitor chemical structure

3.3 Assays

3.3.1 Cell viability assays

10X presto blue (alamar??) was added in a 1:10 ratio to cells in suspension and incubated at 37°C for two to three hours. Plates were read [DETAILS OF MACHINE AND PROTOCOL, e.g. wavelength]

3.3.2 Dose response curves

90µl of cells in fresh media were seeded into 96-well plates a day prior to treatment with compound. A total of 10,000 cells were seeded into each well. No cells were placed in edge wells, to avoid edge effects. The following day, media 0% viability controls were placed in the first and last row. Drug concentrations were made

up 1000x the desired final concentration in eppendorfs. Drugs were diluted 1 in 100 in 96 well round bottom plates with media and then 10µl was added to the 90µl of seeded cells in triplicate. Cells were treated with DMSO in triplicate as 100% viability controls.

3.4 Bulk RNA-seq

3.4.1 RNA extraction

RNA was extracted and purified using the Direct-Zol RNA MiniPrep kit (Zymo, USA), following the manufacturer's protocol. In brief, for each sample, approximately 100,000 cells were lysed in 300µl of TRIzol and the lysate was transferred to a microcentrifuge tube. 300µl of ethanol was added to the lysed samples and vortexed. The mixture was transferred to miniPrep columns and centrifuged at 10,000-16,000g for 30 seconds. The column was washed twice with 400µl of Direct-Zol pre-wash and once with 700µl of RNA wash buffer. The column was transferred to an RNase-free tube and eluted with 50µl of nuclease-free water and centrifuged.

The RNA concentration was quantified using a NanoDrop ND-1000 Spectrophotometer (Thermo Fisher Scientific, USA), and samples were stored at -80°C. Samples were normalised to 100ng with nuclease-free water.

3.4.2 RNA library preparation

NEBNext® Ultra II directional RNA library prep kit for Illumina® with TruSeq indexes was used to prepare RNA libraries, following the manufacturer's protocol. RNA concentration was normalised to 100ng with nuclease-free water, made up to 50µl. The NEBNext Poly(A) mRNA Magnetic Isolation Module (NEB, USA) was used to enrich poly-adenylated RNA. READ booklet in lab

The molarities of the libraries were determined by electrophoresis on a TapeStation (Agilent, USA).

3.5 Single-cell RNA-seq

3.5.1 Cell encapsulation

The Drop-Seq protocol[42] was followed for single-cell RNA-Seq sample preparation. Cells were loaded into a microfluidics cartridge. Nadia, an automated microfluidics device (Dolomite Bio, UK), performed cell capture, cell lysis and reverse transcription. Reverse transcription reactions were performed using ChemGene beads or (ATDBio beads 2020 onwards!!!! might need to change if reperform).

3.5.2 Library preparation

Beads were collected from the device and cDNA amplification was performed. The beads were treated with Exo-I prior to PCR. The amplified, purified cDNA then underwent tagmentation reactions. A TapeStation (Agilent, USA) was used to assess library quality. The samples were pooled together and split across multiple sequencing runs.

3.6 ATAC maybe

3.6.1 ATAC stuff

3.7 ChIP maybe

3.7.1 ChIP stuff

3.8 Sequencing

Sequencing of the resultant libraries was performed on the NextSeq 500 (Illumina, USA) platform using a paired-end run, according to the manufacturer's instructions.

3.9 Phosphoproteomics

3.9.1 Collecting cell pellets

Greater than 20 million cells for each condition (in triplicate) was taken. The cell suspension was centrifuged at 1500g for five minutes. The supernatant was

removed, the pellet was re-suspended in 500µl of ice-cold PBS, transferred to a 1.5ml eppendorf and centrifuged for a further five minutes. The supernatant was removed using a pipette and the pellet was stored at -80°C.

3.9.2 Cell lysis

300µl of fresh lysis buffer (10ml RIPA buffer, 3µl benzonase, 1 tablet phos stop) was added to each pellet, vortexed and left for 10 minutes on ice and then sonicated. The supernatant was transferred to a fresh tube.

3.9.3 Protein quantification

Protein concentrations were determined by BCA protein assay (ThermoFisher, UK). 400µg of protein was taken from each sample. Samples were made up to a volume of 200µl with MilliQ-H₂O.

3.9.4 Protein Digestion

Kessler lab protocols were followed (<https://www.tdi.ox.ac.uk/research/research/tdi-mass-spectrometry-laboratory/mass-spectrometry/protocols-and-tools>).

The lysed samples were reduced with 5µl of 200mM DTT in 0.1 M Tris buffer and incubated for 40 minutes at room temperature. The reduced samples were alkylated with 20µl of 200mM iodoacetamide in 0.1M Tris buffer, vortexed and then incubated for 45 minutes in the dark at room temperature. The protein was precipitated using methanol/chloroform extraction. The alkylated samples were transferred to 2ml eppendorfs. 600µl of methanol was added to each sample, followed by 150µl of chloroform and then vortexed gently. 450µl of MilliQ-H₂O was then added and vortexed gently. The samples were centrifuged at maximum speed on a table top centrifuge for one minute. The upper aqueous phase was removed, without disturbing the precipitate at the interface. 450µl of methanol was added to each sample, without disturbing the disc and centrifuged for two minutes. Protein pellets were resuspended, one sample at a time: the supernatant was removed and 100µl of 6M urea in 0.1M Tris buffer was added. The samples were vortexed and then sonicated (???). Samples

were diluted with 500µl MilliQ-H₂O, to ensure the final urea concentration was below 1M. Porcine trypsin (Sequencing Grade Modified Trypsin; Promega, USA) was added in a 1:50 ratio of enzyme:total protein content of sample, such that 40µl of trypsin solution containing 8µg trypsin in 0.1M Tris buffer was added to each sample. Samples were left to digest overnight at 37°C in an incubator shaker.

3.9.5 Peptide purification

The following day, the reaction was stopped, acidifying samples to 1% Trifluoroacetic acid (TFA). Samples were desalted and concentrated using 1ml C-18 Sep-Pak (Waters) cartridges. Two reagents were used: solution A (98% MilliQ-H₂O, 2% Acetonitrile (CH₃CN) and 0.1% TFA) for washing and solution B (65% Acetonitrile, 35% MilliQ-H₂O and 0.1% TFA) for activation and elution. The columns were flushed with 1ml of solution B and then washed with 1ml of solution A. The digested samples were added to the columns and vacuumed through slowly. Two 1ml washes with solution A were performed. Fresh, labelled eppendorfs were placed beneath the columns and peptides were eluted with 500µl of solution B. For phosphopeptide-enrichment, 90% of the peptides were removed for Immobilized Metal Affinity Chromatography (IMAC) on a Bravo Automated Liquid Handling Platform (Agilent). 10% of the peptides were used for total proteome analysis. Eluted peptides were dried using a vacuum concentrator (Speedvac, Eppendorf) and stored at -20°C until analysis by mass spectrometry (MS). Prior to MS analysis, dried peptides were resuspended in solution A.

3.10 Ubiquitinomics

3.10.1 Collecting cell pellets

100 million cells in triplicate for each condition was taken. The cell suspension was centrifuged at 1500g for five minutes. The supernatant was removed, the pellet was re-suspended in 500µl of ice-cold PBS and centrifuged for a further five minutes. The supernatant was removed and the pellet was stored at -80°C.

3.10.2 Cell lysis

PMTScan Ubiquitin Remnant Motif Kit (K- ϵ -GG; Cell signalling, USA) was used, following the manufacturer's protocol (REF). Pellets were solubilized and denatured in 4ml urea lysis buffer (20mM HEPES, pH 8.0, 9M urea, 1mM sodium orthovanadate, 2.5mM sodium pyrophosphate, 1mM β -glycerophosphate). The lysates were sonicated on ice, with two bursts of 15 seconds with a one minute break in-between.

3.10.3 Protein quantification

Protein concentrations were determined by BCA protein assay (Thermofisher, UK). All samples were found to contain between 10mg and 20mg of protein, so all of the available protein was used, with no normalisation.

3.10.4 Protein Digestion

Lysates were reduced using dithiothreitol (DTT) at a final concentration of 4.5 mM for 30 minutes at room temperature. The reduced samples were alkylated using iodoacetamide (100mM final) for 15 minutes in the dark at room temperature. The alkylated samples were diluted four-fold with 20mM HEPES (pH 8.0) and digested with 400 μ l trypsin solution, containing 1mg ml⁻¹ trypsin-TPCK (Worthington, LS003744) in 1mM HCl. Samples were left to digest overnight at room temperature on a rotator.

3.10.5 Peptide purification

The following day, the reaction was stopped, acidifying samples to 1% Trifluoroacetic acid (TFA). Samples were desalted and concentrated using 10ml C-18 Sep-Pak (Waters) cartridges. The columns were activated using 5ml of solution B, washed with 10ml of solution A. The samples were added to the columns and ran through slowly. The peptides were washed with 10ml of solution A. The cartridges were then removed from the vacuum and the peptides were eluted into fresh falcon tubes with 6ml of solution B, using the plunger of the syringes. 20 μ g of digested

protein was removed from each sample for matching total proteome analysis. The eluate was kept at -80°C overnight. The frozen peptide solutions were lyophilized for two days and then stored at -80°C .

3.10.6 Immunoaffinity purification

10x immunoaffinity purification (IAP) buffer provided with PTMScan Kit was diluted to 1x concentration with MilliQ- H_2O . Purified peptides pellets were resuspended in 1.4ml of IAP buffer by pipetting up and down and transferred to 1.7ml eppendorfs. The samples were centrifuged at 4°C for 5 minutes at 10000xg and kept on ice whilst preparing antibody beads. The anti-body bead slurry was centrifuged (30 seconds at 2000 g) and 1ml of PBS was added and then centrifuged. The supernatant was removed and the antibody beads were washed a further four times with PBS and resuspended in 40 μl of PBS. The peptide solution was transferred to the antibody vial and the solution was incubated on a rotator for two hours at 4°C . The samples were centrifuged, put on ice and the supernatant was removed. The beads were washed twice with 1ml IAP, followed by three washes with 1ml chilled HPLC water. Immunoprecipitated material was eluted at room temperature in 55 μl and 50 μl 0.15% TFA in water, letting the sample stand for 10 minutes after each elution, with gentle mixing every two-three minutes. The eluates were centrifuged and the supernatant was transferred to new tubes. Peptide material was desalted and concentrated using 1ml C-18 Sep-Pak cartridges as above. Prior to mass spectrometry analysis, purified GlyGly-modified peptide eluates and matching proteome material were dried by vacuum centrifugation, and re-suspended in solution A.

3.11 Liquid-chromatography-tandem mass spectrometry

Liquid-chromatography-tandem mass spectrometry (LC-MS/MS) analysis was performed using a Dionex Ultimate 3000 nano-ultra high pressure reverse-phase chromatography coupled on-line to an Orbitrap Fusion Lumos mass spectrometer (Thermo Scientific) (REF: adan's 3-5 dropbox). In brief, samples were separated on

an EASY-Spray PepMap RSLC C18 column (500mm \times 75 μ m, 2 μ m particle size; Thermo Scientific) over a 60 min (120 min in the case of the matching proteome) gradient of 2–35% acetonitrile in 5% dimethyl sulfoxide (DMSO), 0.1% formic acid at 250nlmin⁻¹. MS1 scans were acquired at a resolution of 60000 at m/z 200 and the top 12 most abundant precursor ions were selected for high collision dissociation (HCD) fragmentation.

3.12 Data Processing

3.12.1 Bulk RNA-Seq

Fasta files were processed using a CGAT-flow (REF) pipeline, workflow can be found at: https://github.com/cgat-developers/cgat-flow/blob/master/cgatpipelines/tools/pipeline_rnaseqdiffexpression.py. Pseudo-alignment tool, Kallisto (REF), was implemented to pseudo-align reads to the reference human genome sequence (GRCH38 (hg38) assembly) and to construct a counts matrix of samples against transcripts (/GENES??). DESeq2 (REFERENCE) was used for differential expression analysis of the generated counts matrix (using negative binomial generalized linear models) within the R statistical framework (v3.5.1).

3.12.2 Single-cell RNA-Seq

The computational pipeline outlined in section 4.2 was used to process scRNA data.

3.12.3 LC-MS/MS

Mass-spectrometry raw data were searched against the UniProtKB human sequence data base and label-free quantitation (LFQ) was performed using MaxQuant Software (v1.5.5.1). Digestion was set to trypsin/P. Search parameters were set to include carbamidomethyl (C) as a fixed modification, oxidation (M), deamidation (NQ), and phosphorylation (STY) as variable modifications. A maximum of 2 missed cleavages were allowed for phosphoproteome analysis and 3 for the GlyGly peptidome analysis, with matching between runs. LFQ quantitation was performed using unique peptides only. Label-free interaction data analysis was performed

using Perseus (v1.6.0.2). Results were exported to Microsoft Office Excel Sheets and imported into the R statistical framework (v3.5.1) for further analysis.

3.13 CyTOF

Get data off ADAM

3.13.1 CyTOF stuff

Workflow Generation

4.1 Introduction

4.1.1 Reproducible workflows

In data analysis, particularly in bioinformatics, many users create simple bash or R scripts to execute the specific task at hand. However, if this is done often, the user can have an accumulation of these single-use scripts, which are often named uninformatively and never used again. Subsequently, the user may create scripts which perform the same function numerous times. Additionally, users may just use the command line alone to perform tasks. This means that exactly how they performed the analysis is difficult to find or not recorded. These are bad practices in terms of efficiency and reproducibility. It is much better practice to create well-documented, generalised workflows which can then be applied to multiple different experiments. This enables the user to reuse their code more easily and reproduce results, if need be. This also allows other researchers to reproduce results or apply the code to their own research.

In addition to creating generalised, reproducible workflows, it can be beneficial to create more extensive computational pipelines for jobs which require multiple tasks or actions to be performed sequentially.

4.1.2 Computational pipelines

A computational pipeline consists of a series of manipulations and transformations, where the output of one element is the input of the next. Often these elements are executed in parallel. Pipelining ‘omics’ data-processing means that tasks that are not interdependent can be executed simultaneously. Additionally, multiple samples can be processed in parallel, thereby reducing run time. There are many available pipelining frameworks, for example Snakemake[46], Luigi and Ruffus[47].

For this work, a series of computational pipelines and workflows were generated. Ruffus and CGAT-core[48] were used as the backbone for the pipelines developed.

4.2 scRNA-Seq pseudoalignment pipeline

Fewer pipelines exist for single-cell RNA-Seq compared to bulk RNA-Seq. For the Chromium 10X Genomics platform, most of the processing and analysis is automated by Cell Ranger; however for other technologies, the workflow is not as well defined. A single-cell analysis pipeline was constructed with the aim to produce an easy-to-use, robust and reproducible workflow that works for Drop-Seq as well as 10X technology, which utilises pseudoalignment rather than traditional mapping methods.

4.2.1 Psuedoalignment

Traditional mapping techniques such as Tophat[49] or STAR[50], rely on aligning each read to a reference genome. This is generally very time consuming and computationally expensive. Another challenge that arises with traditional mapping is the occurrence of multi-mapping, whereby a read cannot be uniquely aligned as it could map equally well to multiple sites in the genome[51]. More recently, a series of methods called pseudoaligners have been developed that overcome some of the issues associated with traditional mapping approaches. Pseudoalignment (sometimes referred to as quasi-mapping) methods provide a lightweight, alignment-free alternative to traditional mapping. It has been shown that information on where exactly inside transcripts sequencing reads may have originated is not required for

accurate quantification of transcript abundances[52]. Rather, only which transcript the read could have originated from is needed and transcript abundances are calculated by computing the compatibility of reads with different transcripts. This negates the need for alignment to a reference genome, alleviating the issue of multi-mapping and reducing the computational load. Pseudoaligners have been shown to complete data processing of RNA-seq datasets up to 250-times faster than traditional alignment and quantification approaches[53]. Kallisto[53] and Salmon[54] are tools which implement pseudoalignment. They have similar speed and accuracy for bulk RNA-seq data¹.

Pseudoalignment of scRNA-seq

Pseudoalignment tools have recently been developed for droplet-based scRNA-seq analysis (dscRNA-seq). Additional challenges come with dscRNA-seq data processing, having the extra complication of cellular barcodes (CBs) and unique molecular identifiers (UMIs). These tools must handle transcript abundance estimation, as with bulk RNA-seq analysis, but also perform CB detection, collapsing of UMIs (arising from PCR duplication of molecules) and barcode error correction. Kallisto BUS[55] has been developed as an analysis tool and file format specifically for single-cell analysis, alongside BUStools, for processing of the resultant BUS file[56]. Salmon Alevin[57] has also been developed for single-cell RNA-seq analysis.

Pipeline outline

Kallisto BUS or Salmon Alevin performs pseudoalignment and generation of a cell-by-gene expression counts matrix. Quality control is performed using Scater[58] and alevinQC. Clustering is performed using Seurat3[59] and Monocle[60]. Clusters are projected onto tSNE and UMAP plots. Differentially expressed genes are identified by performing non-parametric Wilcoxon tests on $\log_2 TPM$ expression values and Fisher's exact test for comparing expressing cell frequency, these p values combined using Fisher's method. Multiple comparisons are accounted for by performing the Benjamini-Hochberg correction to adjust the false discovery rate.

¹<https://liorpachter.wordpress.com/2017/09/02/a-rebuttal/>

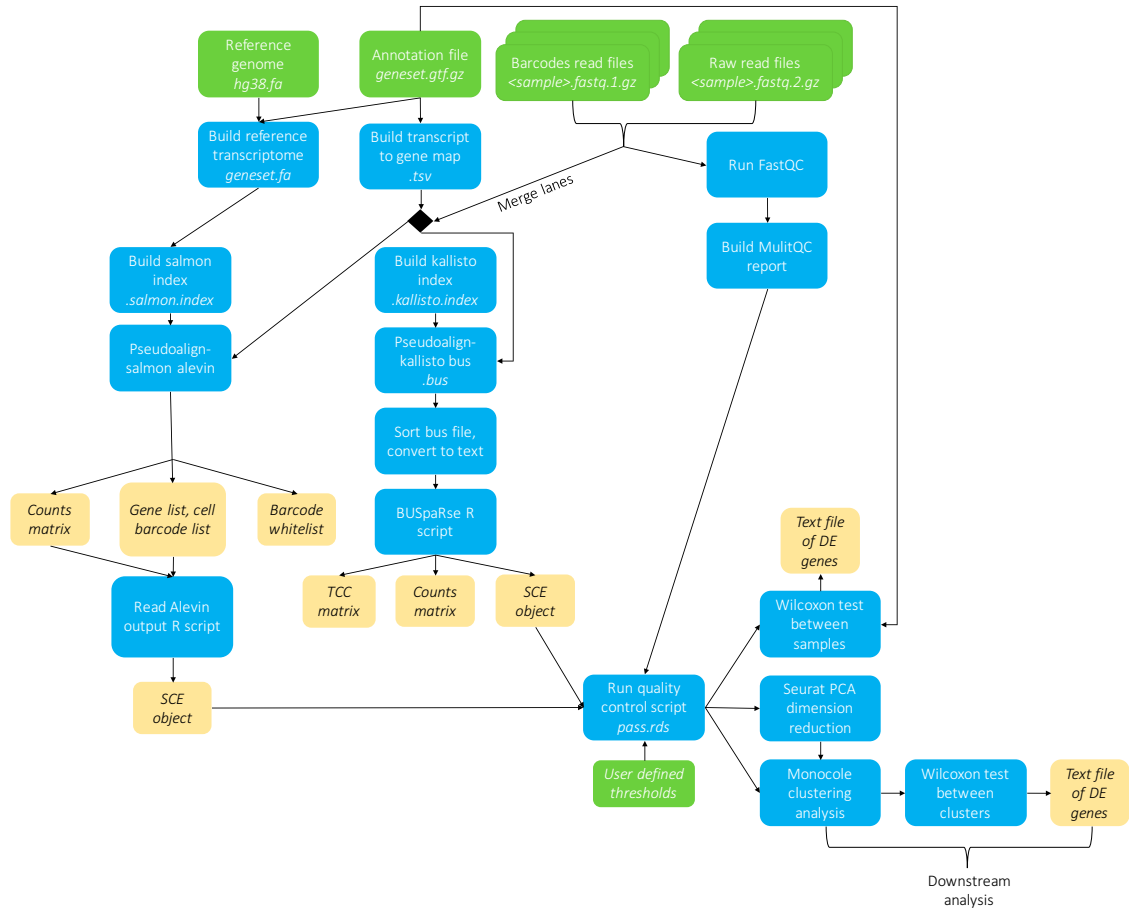


Figure 4.1: Flowchart outlining scRNA-Seq pseudoalignment pipeline- PLACEHOLDER-remake figure

4.2.2 Benchmark

Benchmarking measures the performance of a method/software relative to other methods available. Run time and the accuracy of results are often the factors considered in a benchmark. To be able to calculate the accuracy of results, the ‘true’ results must be known. This is difficult in scRNA-seq analysis as no gold standard analysis protocol exists. Instead, methods are compared against simulated results which act as the underlying ‘ground truth’.

Simulated data

Simulated reads with a know ground truth counts matrix were generated as follows: 10X (version 2) fastq files of 4k PBMCs from a healthy human donor

were downloaded ². These sequencing files were processed using Salmon Alevin. The resulting Alevin output folder was used as input for Minnow, using Minnow’s alevin-mode. Minnow generates droplet-based scRNA-seq simulated reads, working backwards from a known counts matrix to generating raw sequencing files from which the counts matrix could have originated. The valid cell barcode list (whitelist) for 10X chemistry was used (*737K-august-2016.txt*³). Minnow was ran with an error rate of 0.001 and with 12 simulated PCR cycles. Minnow accounts for core experimental dscRNA-seq characteristics, such as PCR amplification bias, barcode sequencing errors, the presence of doublets and ambiguously mapped reads, to try and emulate a realistic set of sequencing reads consistent with the provided counts matrix.

The ground-truth counts matrix was converted to a Single Cell Experiment object (SCE) and the simulated reads were used as input for the scRNA-Seq pseudoalignment pipeline. The resulting count matrices outputted by Salmon Alevin and Kallisto BUS were converted into SCEs, subset and reordered so that they all contained the same cells and genes, in the same order. The Salmon Alevin and Kallisto BUS produced SCEs could then be compared to the ground truth SCE.

Run time

The simulated reads consisted of 434 million reads. Running Salmon Alevin and creating an SCE object took approximately 64 minutes; running Kallisto BUS, sorting and creating an SCE object took approximately 24 minutes. Using the bustools ‘count’ command to create a counts matrix may have further reduced run time, however more time would be needed to parse it into R and create an SCE object.

Cell barcode handling

The ground-truth data contained 4340 cells. Alevin determined a threshold for the initial whitelist (a set of CBs that likely represent non-empty droplets) by finding a

²<https://support.10xgenomics.com/single-cell-gene-expression/datasets>

³<https://github.com/COMBINE-lab/minnow/blob/master/data/737K-august-2016.txt>

‘knee’ in the knee plot shown in Figure 4.2. This initial whitelist contained 5261 cell barcodes, each observed at least 191 times. Following barcode error correction, the final whitelist contained 4340 cells, all of which corresponded to the same CBs as the ground-truth data.

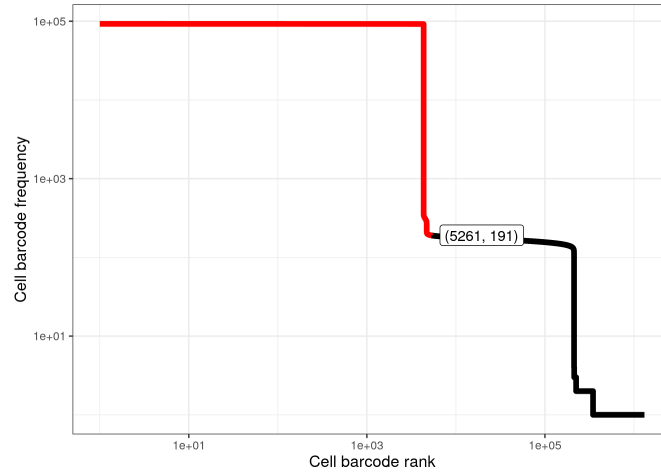


Figure 4.2: Alevin knee plot. This plot displays the number of times each cell barcode is observed, in decreasing order. Finding a ‘knee’ in this plot determines a threshold for the initial whitelist of CBs, which are unlikely to be empty droplets.

For Kallisto BUS, valid cell barcodes were determined using either emptyDrops (DropletUtils) or by using barcodeRanks and calculating the inflection point of a rotated knee plot (where the x- and y- axis are transposed; Figure 4.3). The inflection point method, gave a whitelist of 4339 cell barcodes (one fewer than the ground truth number), but all 4339 CBs corresponded to ground truth CBs. emptyDrops gave a total cell number of 12037, only 3746 of which were in the ground truth list of 4340 CBs. This was a large overestimate of number of cells present and the whitelist did not contain all of the valid CBs. Therefore, using the inflection point of the rotated knee plot was found to be the preferred method of filtering cell barcodes.

Gene expression predictive accuracy

To quantify each tool’s accuracy of gene expression, precision, recall and an F1 score were calculated for each gene. The F1 score is a measure of a test’s accuracy,

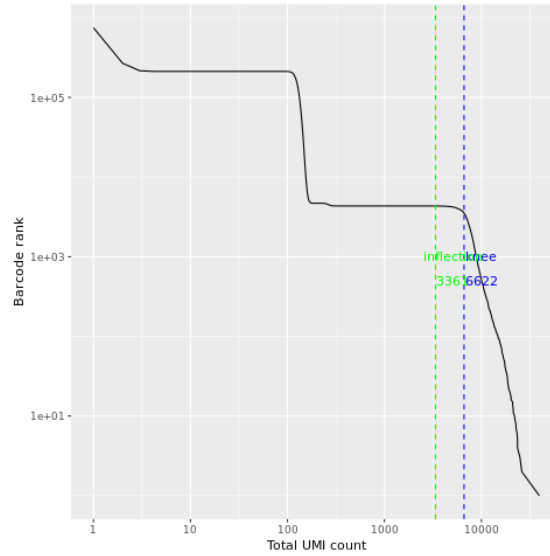


Figure 4.3: Kallisto BUS rotated knee plot. This plot shows the number of distinct UMIs against the rank of the barcode. The Pachter lab transpose the x- and y-axis on their knee plot, so that the x-axis displays distinct UMIs and the y-axis displays ranked cell barcodes, according to the number of corresponding UMIs to each CB. This is supposed to be more intuitive, having the number of distinct UMIs as the independent variable rather than cell barcode rank, as number of UMIs determine the cell barcode rank.

it is the harmonic mean of precision and recall:

$$\begin{aligned}
 \text{precision} &= \frac{tp}{tp + fp} \\
 \text{recall} &= \frac{tp}{tp + fn} \\
 F_1 &= 2 \cdot \frac{\text{precision} \cdot \text{recall}}{\text{precision} + \text{recall}}
 \end{aligned} \tag{4.1}$$

Where for each gene: tp = number of true positives, fp = number of false positives, fn = number of false negatives.

		Ground truth	
		Expressed	Not Expressed
Alevin /BUS	Expressed	True positive	False positive
	Not Expressed	False negative	True negative

Table 4.1: Carol diagram of true/false positives/negatives based on expression between predicted values by Alevin/BUS and the ground truth matrix.

No expression was denoted by 0, and expression by 1. When recall or precision

was undefined, i.e. a gene in Alevin/BUS matrix or the ground-truth matrix was not expressed by any cell, F score was defined as 0.

The mean F1 scores for Alevin and BUS processed data (Figure 4.4) were extremely similar to each other with scores of 0.93 and 0.95, this was due to the large number of F1 scores equal to 1. Figure 4.5 shows the distribution of F1 scores more clearly. Alevin seemed to produce more lower F1 scores than BUS.

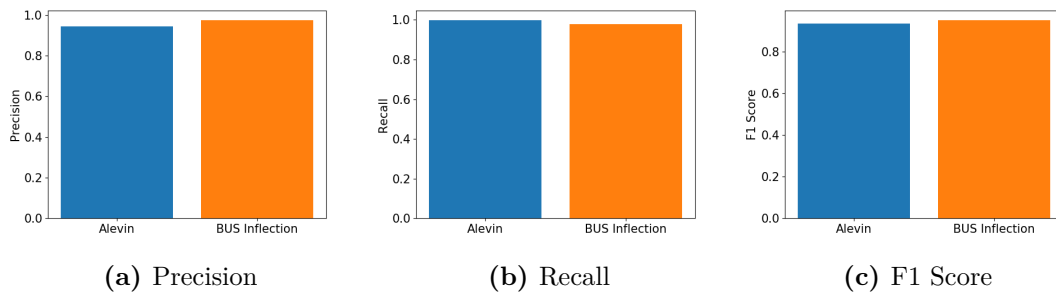


Figure 4.4: F1 score. Two times the product of precision and recall divided by the sum of precision and recall. Measure of accuracy for the tools ability to predict gene expression. Expression classified by 0 or 1. Undefined scores have been removed. F1 scores were calculated for each gene across each cell.

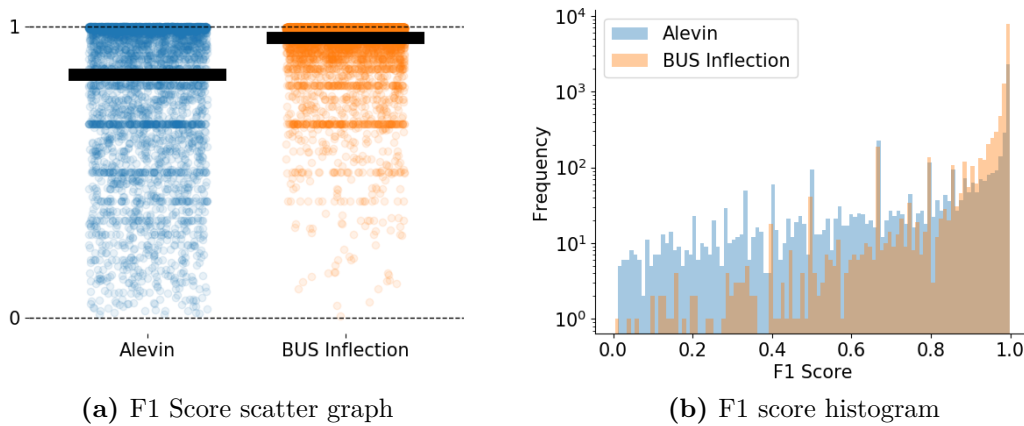


Figure 4.5: F1 score distributions. 4.5a shows the F1 score for each gene expressed across all 4339 cells. The black bar denotes the mean F1 score for each cell. F1 scores of 0 have been removed.

Clustering

Clustering analysis was performed to visualise how well the tools processed the single-cell data and how clusters compared to ground-truth data. Seurat3 integrative

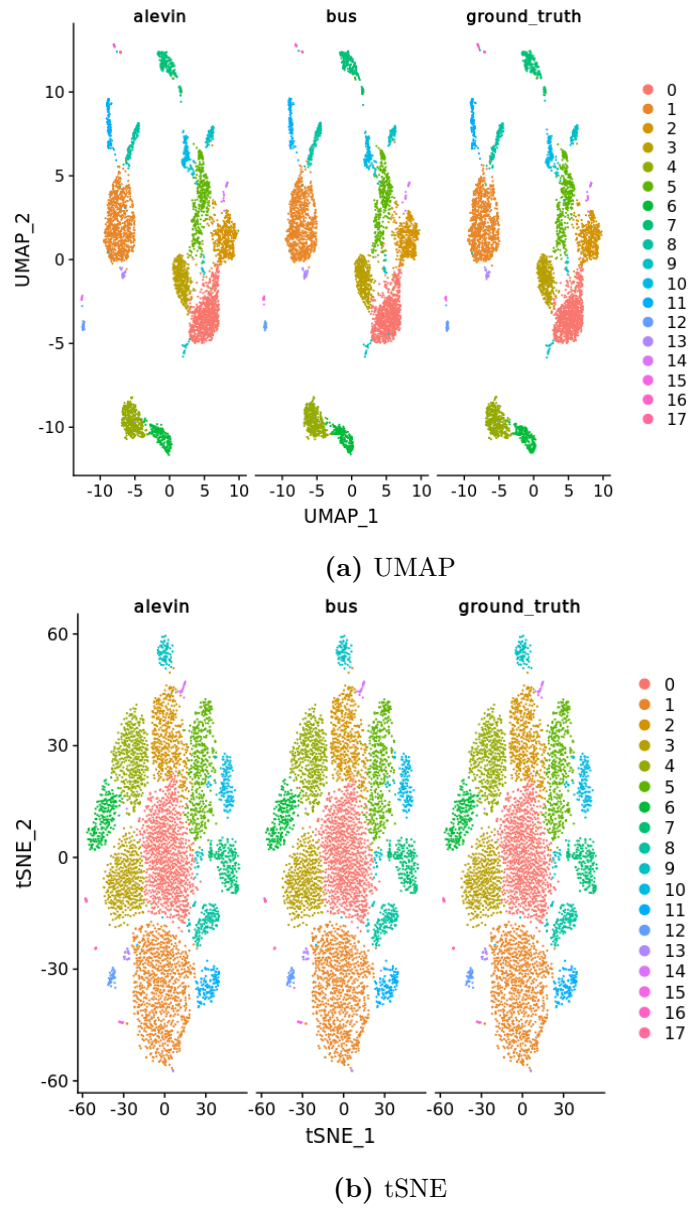


Figure 4.6: Clustering analysis of the simulated data. 18 clusters are present in the ground truth data and Alevin and BUS processed data. Integrated clustering was performed using Seruat3[59], using both Uniform Manifold Approximation and Projection (UMAP) and t-distributed Stochastic Neighbor Embedding (tSNE) dimension reduction techniques.

analysis was performed so that the clusters of each sample could be directly compared. Figure 4.6 shows clustering of Alevin, BUS and ground-truth clustered data, using UMAP and tSNE dimension reductions. 18 clusters are present in all three of the data sets. Visual analysis suggests that the two dscRNA-seq quantification tools compare well to the ground-truth and capture most aspects of the data. From the

benchmark it seems as if both tools are fit for purpose and can accurately quantify gene expression and correctly handle CBs and UMIs.

4.3 scRNA-Seq velocity analysis pipeline

4.3.1 RNA velocity

“RNA velocity is a high-dimensional vector that predicts the future state of individual cells on a timescale of hours”[61]. In combination with clustering analysis, the trajectory of a single-cell can be tracked.

Identifying a lead epigenetic compound

5.1 Identifying inhibitors of interest

Preliminary work in section 2.2 shows an epigenetic compound library screen against PI sensitive and PI resistant AMO-1 cells, in the presence of PI and without PI.

5.1.1 Bulk RNA-seq

Following the compound library screen, a pilot bulk RNA-seq experiment containing WT, aBTZ cells and aCFZ cells in triplicate and single samples of aCFZ and WT cells treated with epigenetic inhibitors, was conducted. Cells were treated for 24 hours with either DMSO for cell-line only controls, or an epigenetic inhibitor, before being harvested for bulk RNA-seq. Following the initial pilot, bulk RNA-seq was performed again with aCFZ cells and aCFZ cells treated with the six epigenetic inhibitors. aCFZ cells were treated with 1 μ M CBP30, TMP269, GSK959 or T54, 5 μ M OF1, or 10 μ M TRIM24i for twenty-four hours, RNA was harvested and bulk RNA-Seq analysis was performed.

I combined the DESeq2 [62] results for the two experiments, transformed the data to be approximately homoskedastic and removed the batch effects of the two separate experiments using the *limma* package [63]. This meant I was able to compare WT cells more easily with aCFZ treated with the epigenetic inhibitors, without performing another costly RNA-seq experiment.

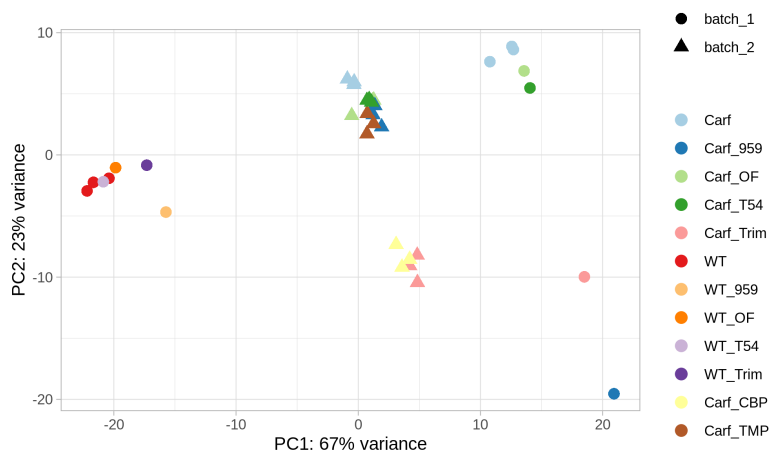


Figure 5.1: PCA plot for two bulk RNA-seq experiments. WT and aCFZ cells treated with compounds GSK959 (959), OF1 (OF), TDOS10000054a (T54), TRIM24/BRPF (TRIM24i), SGC-CBP30 (CBP), TMP269 (TMP) and DMSO controls across two bulk RNA-seq experiments. Batch effects have been removed.

Figure 5.1 shows a PCA plot for the two combined experiments. The first principle component (contributing 67% of the total variance) seems to be separating along cell type, such that WT cells and WT cells treated with the epigenetic inhibitors are clustering together on the left of the graph, whilst aCFZ cells and aCFZ cells treated with epigenetic inhibitors are located towards the middle and right-hand-side of the graph. aCFZ cells treated with the compounds OF-1, T54, TMP269 and GSK959 are closely clustered with control aCFZ cells treated with DMSO. This indicates that aCFZ cells treated with OF-1, T54, TMP269 and GSK959 are extremely similar to aCFZ control cells. CBP30 and TRIM24i treated aCFZ cells however cluster away from DMSO treated aCFZ controls on PC2 (contributing 23% of the total variance). The clustering of epigenetic inhibitors is reflected in differential expression analysis. 498 genes were differentially expressed (DE) between CBP30 treated aCFZ cells and DMSO treated aCFZ controls. TRIM24i treated aCFZ cells

had 579 DE genes compared with aCFZ controls. T54 treated aCFZ cells had 19 DE genes, TMP269 treated aCFZ cells had 4 DE genes, GSK959 treated aCFZ cells had 1 DE gene and OF1 treated aCFZ cells had 0 DE genes compared to controls. At the concentrations used, CBP30 and TRIM24i had a larger transcriptional effect on carfilzomib resistant cells than the other four inhibitors. This allows us to examine the mechanism of action of these drugs in more detail, with richer data available. CBP30 and TRIM24i were chosen to take further.

5.1.2 Dose response curves

The results of the compound screen were validated further by creating dose response curves. Firstly WT, aCFZ and aBTZ cells were treated with carfilzomib and bortezomib, to validate sensitivity to PI (Figure 5.2a). [MORE DOSE REPSONSE CURVES– aBTZ and aCFZ and WT for batch 1 and batch 2 with bort and carf] At concentrations above 20nM WT cells were being killed by carfilzomib. IC₅₀s of WT, aCFZ and aBTZ cells to carfilzomib and bortezomib are shown in Table 5.1.

[REDO FOR BTZ]

Cell line	Drug	IC ₅₀ (nM)
WT	Carfilzomib	7.93
	Bortezomib	3.74
aCFZ	Carfilzomib	673
	Bortezomib	174.8
aBTZ	Carfilzomib	827.1
	Bortezomib	402.5

Table 5.1: IC₅₀s of WT, aCFZ and aBTZ cells to carfilzomib and bortezomib.

Next, concentrations of TRIM24i and CBP30 were varied against aCFZ, aBTZ and WT cells, in the presence of carfilzomib or bortezomib and without. Carfilzomib and bortezomib were kept at 25nM as at this concentration WT cells were killed by PI, hence it indicates re-sensitisation to PI at WT levels if killed at this concentration.

Figure 5.2 shows dose response curves for WT and aCFZ cells with carfilzomib and TRIM24/BRP inhibitor. AMO-1 cells were treated for 48 hours with varying carfilzomib concentrations from 1nM to 500nM. Concentrations were too low

to elicit a response in aCFZ resistant cells. The IC_{50} value for WT cells with carfilzomib was 8.39nM.

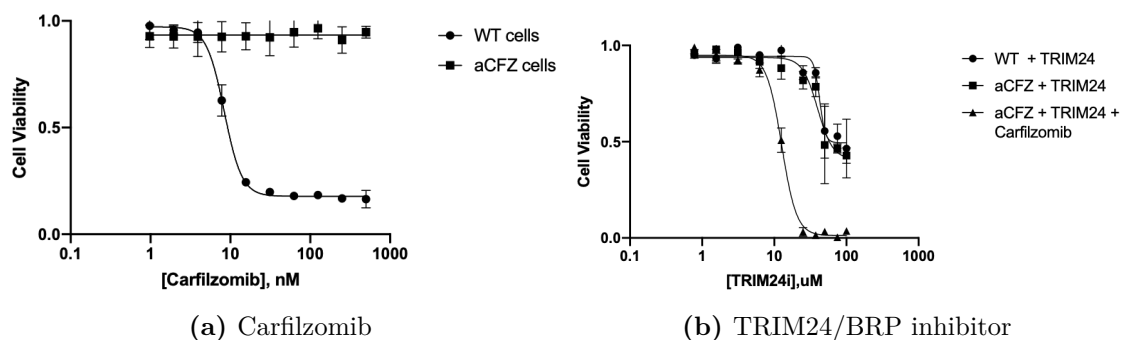


Figure 5.2: Dose response curves. 5.2a shows WT and aCFZ cell viability with varying carfilzomib concentration from 1nM to 500nM. 5.2b shows WT and aCFZ cell viability with varying TRIM24/BRP inhibitor concentration from 0.78 μ M to 100 μ M with and without carfilzomib present (25nM; WT cells died in the presence of carfilzomib).

Thirdly, aCFZ cells were pretreated with 20 μ M TRIM24i for 24 hours and then concentrations of PI were varied (Figure 5.3). The IC_{50} for aCFZ cells pretreated with 20 μ M TRIM24i for carfilzomib was 14.95 μ M and for bortezomib was 35.45 μ M. TRIM24i re-sensitises aCFZ cells to both carfilzomib and bortezomib, however with a larger effect for carfilzomib.

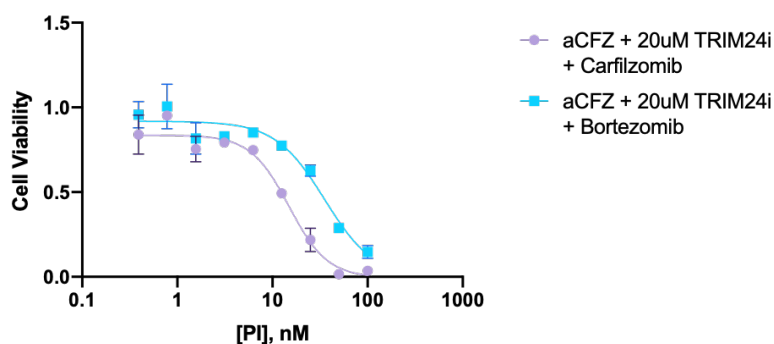


Figure 5.3: Dose response curve for carfilzomib and bortezomib for aCFZ cells pre-treated for 24 hours with TRIM24i.

6

Multi-omics characterisation of PI resistance in AMO-1 cells

6.1 Introduction

Numerous transcriptional changes have been implicated in the development of acquired drug-resistance in MM. It is also pertinent to ascertain if the changes seen in the transcriptome are reflected in protein expression. Therefore both transcriptional changes and proteomic changes must be studied.

The changes between PI-sensitive (WT) AMO-1 cells and PI-resistant (aCFZ/aBTZ) AMO-1 cells will be looked at. In addition, the BRPF1B/TRIM24 dual inhibitor (TRIM24i) was shown in the previous chapter to effectively kill carfilzomib resistant AMO-1 cells in the presence of carfilzomib (but not without carfilzomib), whilst not affecting WT AMO-1 cells. Thus suggesting TRIM24i has a mechanism of action that is capable of reversing aCFZ cells' resistance, and re-sensitising them to carfilzomib again. aCFZ cells treated with TRIM24i will be compared to control aCFZ cells, to better understand the mechanism of action of TRIM24i. Furthermore, these changes must be compared to the differences seen between WT and aCFZ cells. Considering TRIM24i seems to make aCFZ cells sensitive to carfilzomib again, it may be the case that it is reversing some of the changes seen between WT and aCFZ cells.

6.2 Results

6.2.1 Transcriptional changes

To investigate the transcriptional changes that underlie the development of acquired-PI-resistance in multiple myeloma a number of RNA-seq experiments to compare WT, carfilzomib resistant (aCFZ) and bortezomib (aBTZ) AMO-1 cells were performed, both at the bulk and single-cell level.

Principle component analysis (PCA) showed differential clustering of the different cell lines... [PCA of different cell lines, WT, aCFZ, aBTZ]

xyz differentially expressed genes (DEGs) were identified between WT and aCFZ cells.

TRIM24i reversal

To investigate how TRIM24i reverses the resistance phenotype in aCFZ cells, bulk RNA-seq was employed. aCFZ cells (100nM carfilzomib) were treated with DMSO or 10 μ M TRIM24i (in triplicate). The results from this experiment were compared against the results from the previous bulk-RNA experiment of WT controls vs aCFZ cells (100nM carfilzomib).

As seen in figure 6.1, PCA and sample-sample clustering shows TRIM24i treated aCFZ cells clustering away from aCFZ controls. The sample-sample clustering shows TRIM24i treated aCFZ cells clustering closer to WT cells than the aCFZ controls are, suggesting the TRIM24i treatment has made them more similar to WT cells, agreeing with our hypothesis following the dose-response curve results.

Next, transcription factors (TFs) were explored. Figure 6.2 shows a heatmap for DE ($p \leq 0.01$) transcription factors between aCFZ controls and TRIM24i treated aCFZ cells. Figure 6.3 shows a venn diagram for differentially expressed ($p \leq 0.01$) TFs. Transcription factors whose expression have been ‘reversed’ by TRIM24i treatment (i.e. TFs that are up-regulated in aCFZ cells compared to WT, and down-regulated in TRIM24i treated aCFZ cells compared to aCFZ controls, and vice versa) are highlighted in the intersection of the venn diagrams.

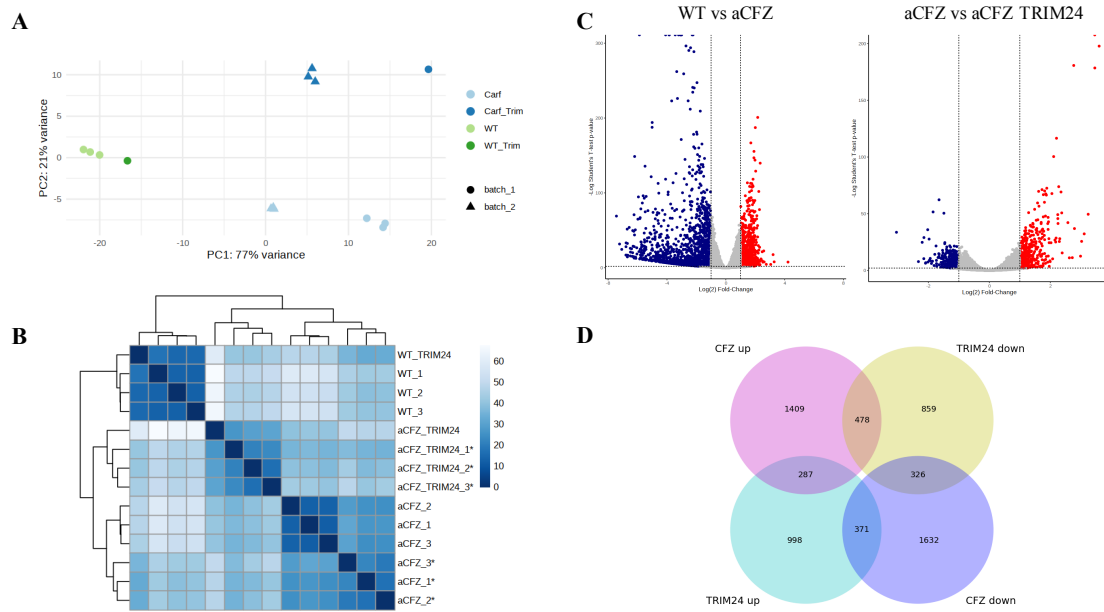


Figure 6.1: **A** shows a PCA plot for WT AMO-1 cells, aCFZ cells (100nM carfilzomib) and aCFZ (100nM carfilzomib) cells treated with 10 μ M TRIM24i. **B** shows a heatmap of sample-sample distances using hierarchical clustering of the samples. **C** shows volcano plots (\log_2 fold change vs $-\log_{10}$ Student's T-test p -value) for WT vs aCFZ AMO-1 cells (100nM carfilzomib) and for aCFZ cells (100nM carfilzomib) vs aCFZ cells (100nM carfilzomib) treated with 10 μ M TRIM24i. **D** shows a four-way venn diagram for differentially expressed genes ($|\log_2 FC| \geq 0.5$), either up-regulated or down-regulated, between WT and aCFZ cells (CFZ) or aCFZ cells and aCFZ cells treated with TRIM24i (TRIM24).

6.2.2 Phosphoproteomics

Phosphoproteomics was performed (method outlined in section 3.9). Five conditions were investigated: WT, aCFZ (+100nM carfilzomib), aCFZ treated with TRIM24 inhibitor (+100nM carfilzomib), aCFZ treated with TRIM24 inhibitor (no carfilzomib), and WT treated with TRIM24 inhibitor.

6.2.3 Ubiquitinomics

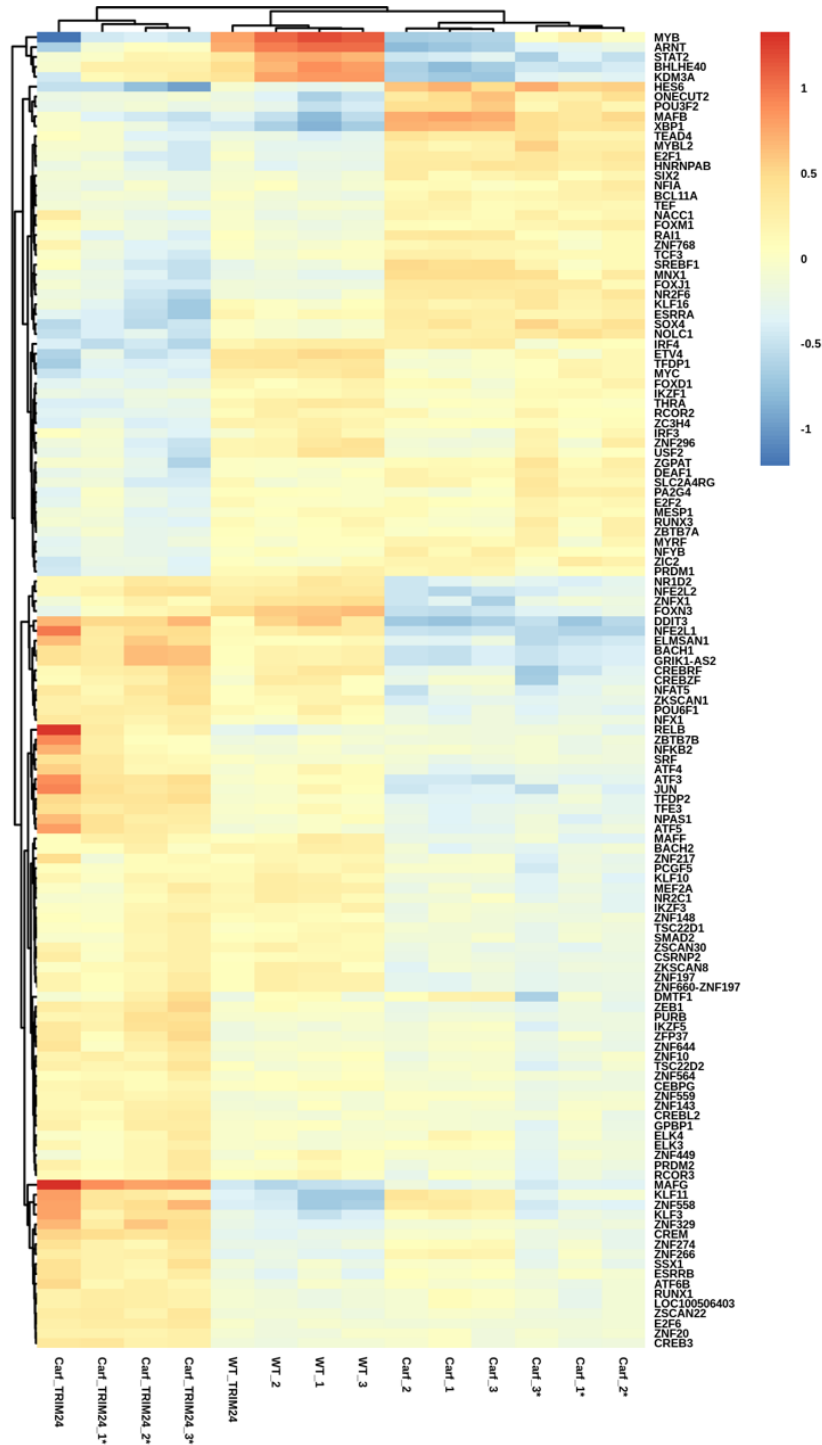


Figure 6.2: Transcription factor heatmap. Variance stabilised expression of transcription factors differentially expressed ($p \leq 0.01$) between aCFZ controls and TRIM24i treated aCFZ cells are shown for WT cells, aCFZ controls and TRIM24i treated aCFZ cells. Samples from experiment 2 have an asterisk (*) next to them, samples from experiment 1 have no asterisk. Batch effects have been removed between experiments

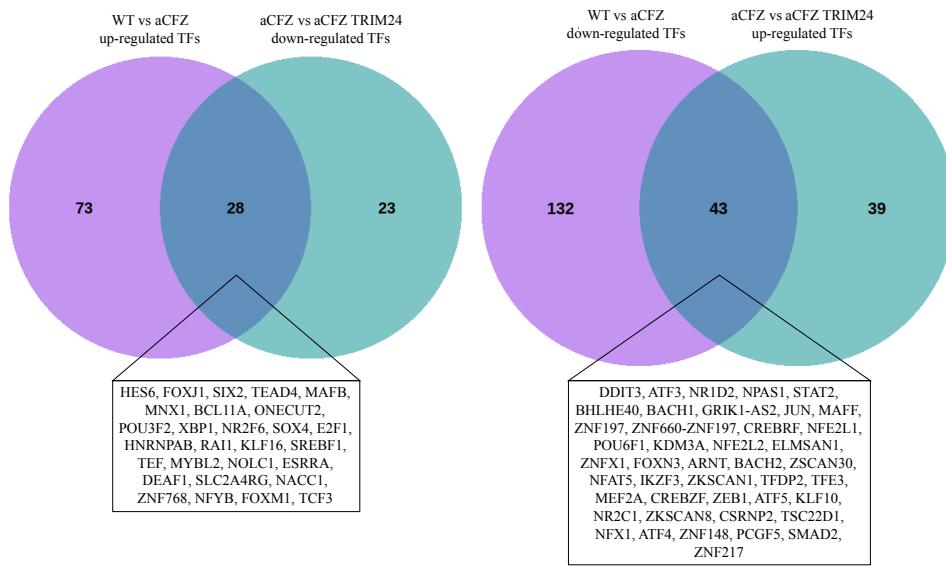


Figure 6.3: **A** shows a PCA plot for WT AMO-1 cells, aCFZ cells (100nM carfilzomib) and aCFZ (100nM carfilzomib) cells treated with 10 μ M TRIM24i. **B** shows a heatmap of sample-sample distances using hierarchical clustering of the samples. **C** shows volcano plots (\log_2 fold change vs $-\log_{10}$ Student's T-test p -value) for WT vs aCFZ AMO-1 cells (100nM carfilzomib) and for aCFZ cells (100nM carfilzomib) vs aCFZ cells (100nM carfilzomib) treated with 10 μ M TRIM24i. **D** shows a four-way venn diagram for differentially expressed genes ($|\log_2 FC| \geq 0.5$), either up-regulated or down-regulated, between WT and aCFZ cells (CFZ) or aCFZ cells and aCFZ cells treated with TRIM24i (TRIM24).

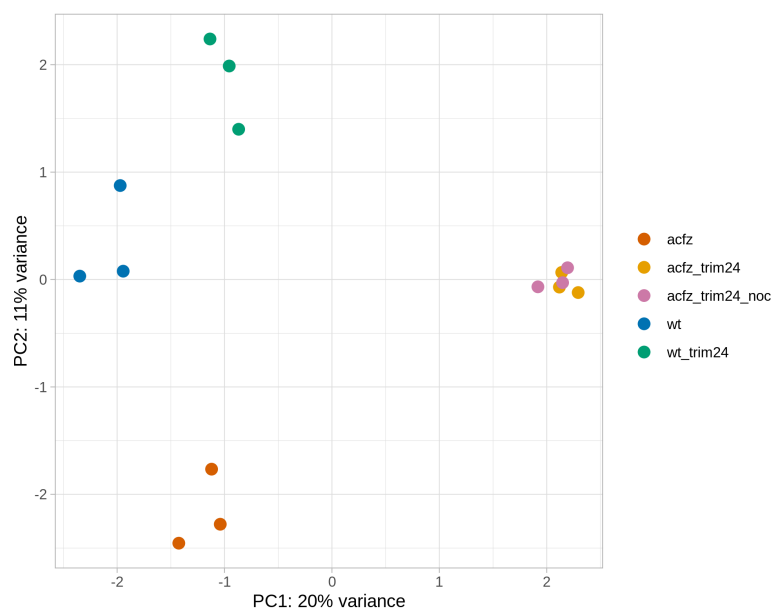


Figure 6.4: PCA plot for phosphoproteomic data. WT, WT treated with TRIM24i, aCFZ + 100nM carfilzomib, aCFZ treated with 10 μ M TRIM24i and 100nM carfilzomib, and aCFZ treated with 10 μ M TRIM24i and no carfilzomib.

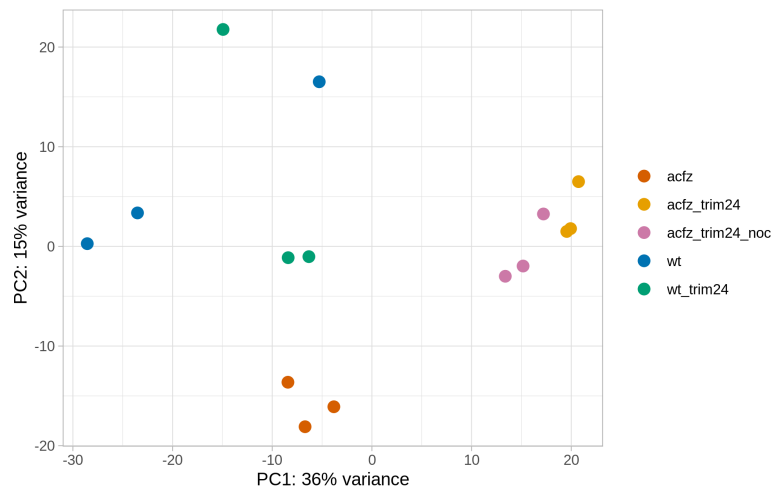


Figure 6.5: PCA plot for Ubiquitinomics data. WT, WT treated with TRIM24i, aCFZ + 100nM carfilzomib, aCFZ treated with 10 μ M TRIM24i and 100nM carfilzomib, and aCFZ treated with 10 μ M TRIM24i and no carfilzomib.

Appendices

A

Epigenetic compound screen

A compound screen consisting of approximately 140 epigenetic inhibitors was performed for AMO-1 cells.

References

- [1] Katrin Roth et al. “Tracking plasma cell differentiation and survival”. In: *Cytometry Part A* 85.1 (2014), pp. 15–24.
- [2] Michel Jourdan et al. “Characterization of a transitional preplasmablast population in the process of human B cell to plasma cell differentiation”. In: *The Journal of Immunology* 187.8 (2011), pp. 3931–3941.
- [3] Miriam Shapiro-Shelef and Kathryn Calame. “Plasma cell differentiation and multiple myeloma”. In: *Current opinion in immunology* 16.2 (2004), pp. 226–234.
- [4] Alexandra Bortnick and David Allman. “What Is and What Should Always Have Been: Long-Lived Plasma Cells Induced by T Cell–Independent Antigens”. In: *The Journal of Immunology* 190.12 (2013), pp. 5913–5918.
- [5] Mathieu Andraud et al. “Living on three time scales: the dynamics of plasma cell and antibody populations illustrated for hepatitis a virus”. In: *PLoS Comput Biol* 8.3 (2012), e1002418.
- [6] Kenneth C Anderson and Ruben D Carrasco. “Pathogenesis of myeloma”. In: *Annual Review of Pathology: Mechanisms of Disease* 6 (2011), pp. 249–274.
- [7] International Myeloma Working Group. “Criteria for the classification of monoclonal gammopathies, multiple myeloma and related disorders: a report of the International Myeloma Working Group”. In: *British journal of haematology* 121.5 (2003), pp. 749–757.
- [8] Matthew Tsang et al. “Multiple myeloma epidemiology and patient geographic distribution in Canada: a population study”. In: *Cancer* (2019).
- [9] Antonio Palumbo and Kenneth Anderson. “Multiple Myeloma”. In: *New England Journal of Medicine* 364.11 (2011), pp. 1046–1060.
- [10] NHS UK. *Multiple Myeloma*.
<https://www.nhs.uk/conditions/multiple-myeloma/>. Accessed: 06-2019.
- [11] Lauren R Teras et al. “2016 US lymphoid malignancy statistics by World Health Organization subtypes”. In: *CA: a cancer journal for clinicians* 66.6 (2016), pp. 443–459.
- [12] Andrew J Cowan et al. “Global burden of multiple myeloma: a systematic analysis for the Global Burden of Disease Study 2016”. In: *JAMA oncology* 4.9 (2018), pp. 1221–1227.
- [13] Cancer Research UK. *Myeloma Survival Statistics*.
<https://www.cancerresearchuk.org/health-professional/cancer-statistics/statistics-by-cancer-type/myeloma/survival>. Accessed: 06-2019.

- [14] Rebecca L Siegel, Kimberly D Miller, and Ahmedin Jemal. “Cancer statistics, 2016”. In: *CA: a cancer journal for clinicians* 66.1 (2016), pp. 7–30.
- [15] Niels van Nieuwenhuijzen et al. “From MGUS to multiple myeloma, a paradigm for clonal evolution of premalignant cells”. In: *Cancer research* 78.10 (2018), pp. 2449–2456.
- [16] S Vincent Rajkumar, Ola Landgren, and Maria-Victoria Mateos. “Smoldering multiple myeloma”. In: *Blood, The Journal of the American Society of Hematology* 125.20 (2015), pp. 3069–3075.
- [17] Neha Korde, Sigurdur Y Kristinsson, and Ola Landgren. “Monoclonal gammopathy of undetermined significance (MGUS) and smoldering multiple myeloma (SMM): novel biological insights and development of early treatment strategies”. In: *Blood* 117.21 (2011), pp. 5573–5581.
- [18] Robert A Kyle et al. “Clinical course and prognosis of smoldering (asymptomatic) multiple myeloma”. In: *New England Journal of Medicine* 356.25 (2007), pp. 2582–2590.
- [19] S Vincent Rajkumar et al. “International Myeloma Working Group updated criteria for the diagnosis of multiple myeloma”. In: *The lancet oncology* 15.12 (2014), e538–e548.
- [20] Dickran Kazandjian and Ola Landgren. “A look backward and forward in the regulatory and treatment history of multiple myeloma: approval of novel-novel agents, new drug development, and longer patient survival”. In: *Seminars in oncology*. Vol. 43. 6. Elsevier. 2016, pp. 682–689.
- [21] N Blokhin et al. “Clinical experiences with sarcolysin in neoplastic diseases”. In: *Annals of the New York Academy of Sciences* 68.3 (1958), pp. 1128–1132.
- [22] ROBERT E MASS. “A comparison of the effect of prednisone and a placebo in the treatment of multiple myeloma.” In: *Cancer chemotherapy reports* 16 (1962), p. 257.
- [23] Raymond Alexanian et al. “Treatment for multiple myeloma: combination chemotherapy with different melphalan dose regimens”. In: *Jama* 208.9 (1969), pp. 1680–1685.
- [24] TJ McElwain and RL Powles. “High-dose intravenous melphalan for plasma-cell leukaemia and myeloma”. In: *The Lancet* 322.8354 (1983), pp. 822–824.
- [25] Elliott F Osserman et al. “Identical twin marrow transplantation in multiple myeloma”. In: *Acta haematologica* 68.3 (1982), pp. 215–223.
- [26] Alexander Fefer, Martin A Cheever, and Philip D Greenberg. “Identical-twin (syngeneic) marrow transplantation for hematologic cancers”. In: *Journal of the National Cancer Institute* 76.6 (1986), pp. 1269–1273.
- [27] G Gahrton et al. “Bone marrow transplantation in multiple myeloma: report from the European Cooperative Group for Bone Marrow Transplantation”. In: *Blood* 69.4 (1987), pp. 1262–1264.
- [28] Robert C Kane et al. “Velcade®: US FDA approval for the treatment of multiple myeloma progressing on prior therapy”. In: *The oncologist* 8.6 (2003), pp. 508–513.
- [29] Paul G Richardson et al. “A phase 2 study of bortezomib in relapsed, refractory myeloma”. In: *New England Journal of Medicine* 348.26 (2003), pp. 2609–2617.

- [30] Alla Katsnelson. *Next-generation proteasome inhibitor approved in multiple myeloma*. 2012.
- [31] Seema Singhal et al. “Antitumor activity of thalidomide in refractory multiple myeloma”. In: *New England Journal of Medicine* 341.21 (1999), pp. 1565–1571.
- [32] FDA Label. “Revlimid-lenalidomide capsule”. In: *For Multiple Myeloma Myelodysplastic Syndrome and Mantle Cell Lymphoma* 47 ().
- [33] Jesus San Miguel et al. “Pomalidomide plus low-dose dexamethasone versus high-dose dexamethasone alone for patients with relapsed and refractory multiple myeloma (MM-003): a randomised, open-label, phase 3 trial”. In: *The lancet oncology* 14.11 (2013), pp. 1055–1066.
- [34] Henk M Lokhorst et al. “Targeting CD38 with daratumumab monotherapy in multiple myeloma”. In: *New England Journal of Medicine* 373.13 (2015), pp. 1207–1219.
- [35] Sagar Lonial et al. “Elotuzumab therapy for relapsed or refractory multiple myeloma”. In: *New England Journal of Medicine* 373.7 (2015), pp. 621–631.
- [36] Jesús F San Miguel et al. “Bortezomib plus melphalan and prednisone for initial treatment of multiple myeloma”. In: *New England Journal of Medicine* 359.9 (2008), pp. 906–917.
- [37] Philippe Moreau et al. “Proteasome inhibitors in multiple myeloma: 10 years later”. In: *Blood* 120.5 (2012), pp. 947–959.
- [38] Gary Kleiger and Thibault Mayor. “Perilous journey: a tour of the ubiquitin–proteasome system”. In: *Trends in cell biology* 24.6 (2014), pp. 352–359.
- [39] Bruce Alberts et al. *Molecular biology of the cell*. 6th ed. Garland science, Dec. 2014, pp. 356–359.
- [40] Fuchou Tang et al. “mRNA-Seq whole-transcriptome analysis of a single cell”. In: *Nature methods* 6.5 (2009), pp. 377–382.
- [41] Simone Picelli et al. “Smart-seq2 for sensitive full-length transcriptome profiling in single cells”. In: *Nature methods* 10.11 (2013), pp. 1096–1098.
- [42] Evan Z Macosko et al. “Highly parallel genome-wide expression profiling of individual cells using nanoliter droplets”. In: *Cell* 161.5 (2015), pp. 1202–1214.
- [43] Saiful Islam et al. “Characterization of the single-cell transcriptional landscape by highly multiplex RNA-seq”. In: *Genome research* 21.7 (2011), pp. 1160–1167.
- [44] Allon M Klein et al. “Droplet barcoding for single-cell transcriptomics applied to embryonic stem cells”. In: *Cell* 161.5 (2015), pp. 1187–1201.
- [45] GP Soriano et al. “Proteasome inhibitor-adapted myeloma cells are largely independent from proteasome activity and show complex proteomic changes, in particular in redox and energy metabolism”. In: *Leukemia* 30.11 (2016), pp. 2198–2207.
- [46] Johannes Köster and Sven Rahmann. “Snakemake—a scalable bioinformatics workflow engine”. In: *Bioinformatics* 28.19 (2012), pp. 2520–2522.
- [47] Leo Goodstadt. “Ruffus: a lightweight Python library for computational pipelines”. In: *Bioinformatics* 26.21 (2010), pp. 2778–2779.

- [48] Adam P Cribbs et al. “CGAT-core: a python framework for building scalable, reproducible computational biology workflows”. In: *F1000Research* 8 (2019).
- [49] Cole Trapnell, Lior Pachter, and Steven L Salzberg. “TopHat: discovering splice junctions with RNA-Seq”. In: *Bioinformatics* 25.9 (2009), pp. 1105–1111.
- [50] Alexander Dobin et al. “STAR: ultrafast universal RNA-seq aligner”. In: *Bioinformatics* 29.1 (2013), pp. 15–21.
- [51] Ali Mortazavi et al. “Mapping and quantifying mammalian transcriptomes by RNA-Seq”. In: *Nature methods* 5.7 (2008), p. 621.
- [52] Marius Nicolae et al. “Estimation of alternative splicing isoform frequencies from RNA-Seq data”. In: *International Workshop on Algorithms in Bioinformatics*. Springer, 2010, pp. 202–214.
- [53] Nicolas L Bray et al. “Near-optimal probabilistic RNA-seq quantification”. In: *Nature biotechnology* 34.5 (2016), p. 525.
- [54] Rob Patro et al. “Salmon provides fast and bias-aware quantification of transcript expression”. In: *Nature methods* 14.4 (2017), p. 417.
- [55] Páll Melsted, Vasilis Ntranos, and Lior Pachter. “The barcode, UMI, set format and BUSTools”. In: *bioRxiv* (2018), p. 472571.
- [56] Páll Melsted et al. “Modular and efficient pre-processing of single-cell RNA-seq”. In: *BioRxiv* (2019), p. 673285.
- [57] Avi Srivastava et al. “Alevin efficiently estimates accurate gene abundances from dscRNA-seq data”. In: *Genome biology* 20.1 (2019), p. 65.
- [58] Davis J McCarthy et al. “Scater: pre-processing, quality control, normalization and visualization of single-cell RNA-seq data in R”. In: *Bioinformatics* 33.8 (2017), pp. 1179–1186.
- [59] Tim Stuart et al. “Comprehensive Integration of Single-Cell Data”. In: *Cell* (2019).
- [60] Cole Trapnell et al. “The dynamics and regulators of cell fate decisions are revealed by pseudotemporal ordering of single cells”. In: *Nature biotechnology* 32.4 (2014), p. 381.
- [61] Gioele La Manno et al. “RNA velocity of single cells”. In: *Nature* 560.7719 (2018), p. 494.
- [62] Michael I Love, Wolfgang Huber, and Simon Anders. “Moderated estimation of fold change and dispersion for RNA-seq data with DESeq2”. In: *Genome biology* 15.12 (2014), p. 550.
- [63] Gordon K Smyth. “Limma: linear models for microarray data”. In: *Bioinformatics and computational biology solutions using R and Bioconductor*. Springer, 2005, pp. 397–420.